Rapid mass growth and enhanced light extinction of atmospheric aerosols during the heating season haze episodes in Beijing revealed by aerosol-chemistry-radiation-boundary layer interaction

Zhuohui Lin[1], Yonghong Wang[2,3], Feixue Zheng[1],Ying Zhou[1],Yishuo Guo[1], Zemin Feng[1], Chang Li[1], Yusheng Zhang[1], Simo Hakala[2], Tommy Chan[2], Chao Yan[2], Kaspar R. Daellenbach[2], Biwu Chu[3], Lubna Dada[2], Juha Kangasluoma[1,2], Lei Yao[2], Xiaolong Fan[1], Wei Du[2], Jing Cai[2], Runlong Cai[2], Tom V. Kokkonen[2,4], Putian Zhou[2], Lili Wang[5], Tuukka Petäjä[2,4], Federico Bianchi[1,2],Veli-Matti Kerminen[2,4],Yongchun Liu[1], and Markku Kulmala[1,2,4]

[1]Aerosol and Haze Laboratory, Beijing Advanced Innovation Center for Soft Matter Science and Engineering, Beijing University of Chemical Technology, Beijing, China

[2]Institute for Atmospheric and Earth System Research / Physics, Faculty of Science, University of Helsinki, Finland

[3]Research Center for Eco-Environmental Sciences, Chinese Academy of Science, Beijing, China

[4]Joint international research Laboratory of Atmospheric and Earth SysTem sciences (JirLATEST), Nanjing University, Nanjing, China

[5]State Key Laboratory of Atmospheric Boundary Layer Physics and Atmospheric Chemistry (LAPC), Institute of Atmospheric Physics, Chinese Academy of Sciences, Beijing 100029, China

Corresponding author: Yonghong Wang

E-mail: yonghongwang@rcees.ac.cn

Revised to: Atmospheric Chemistry and Physics

Abstract

Despite the numerous studies investigating haze formation mechanism in China, it is still puzzling that intensive haze episodes could form within hours directly following relatively clean periods. Haze has been suggested to be initiated by the variation of meteorological parameters and then to be substantially enhanced by aerosol-radiation-boundary layer feedback. However, knowledge on the detailed chemical processes and the driving factors for extensive aerosol mass accumulation during the feedback is still scarce. Here, the dependency of the aerosol number size distribution, mass concentration and chemical composition on the daytime mixing layer height (MLH) in urban Beijing is investigated. The size distribution and chemical composition-resolved dry aerosol light extinction is also explored. The results indicate that the aerosol mass concentration and fraction of nitrate increased dramatically when the MLH decreased from high to low conditions, corresponding to relatively clean and polluted conditions, respectively. Particles having their dry diameters in the size of ~400-700 nm, and especially particle-phase ammonium nitrate and liquid water, contributed greatly to visibility degradation during the winter haze periods. The dependency of aerosol composition on the MLH revealed that ammonium nitrate and aerosol water content increased the most during low MLH conditions, which may have further triggered enhanced formation of sulphate and organic aerosol via heterogeneous reactions. As a result, more sulphate, nitrate and water soluble organics were formed, leading to an enhanced water uptake ability and increased light extinction by the aerosols. The results of this study contribute towards a more detailed understanding of the aerosol-chemistry-radiation-boundary layer feedback that is likely to be responsible for explosive aerosol mass growth events in urban Beijing.

1. Introduction

Despite the recent reduction of air pollutants and their precursors in China between 2013 and 2017, the current emission and air pollution levels are still substantially high (Wang et al., 2020b; Zheng et al., 2018). Such high emissions, combined with specific meteorological conditions, frequently lead to severe haze episodes (An et al., 2019; Wang et al., 2019). Particulate matter, a major air pollutant, has considerable effects on climate, human health and visibility degradation (Che et al., 2007; Lelieveld et al., 2015; Spracklen et al., 2008; Wang et al., 2015).

During winter haze episodes, a rapid growth of the aerosol mass concentration has commonly been observed, and this phenomenon seems to be directly affected by meteorological factors (Li et al., 2018b; Liu et al., 2018, 2019b; Wang et al., 2018a, 2014a). The meteorological conditions and increased aerosol concentrations are proposed to be interlinked by a feedback loop, called the aerosol-chemistry-boundary layer feedback, in which aerosol particles reduce both solar radiation reaching the surface and turbulent kinetic energy (TKE)of the near-surface air (Ding et al., 2016; Petäjä et al., 2016; Wang et al., 2020d).The reduced TKE owing to aerosol reduce the entrainment of relatively dry air into the mixing layer from above, which makes the air more humid within the mixing layer. The increased relative humidity due to decreased surface temperature enhance the aerosol water uptake ability and promote secondary aerosol formation via aqueous-phase reactions, enhancing light scattering and causing further reduction of solar radiation reaching the surface. All of these factors lead to increased stability of mixing layer height and enhanced air pollution in the mixed layer, which further suppresses the development of boundary layer. As a consequence, concentrations of primary aerosol particles, water vapor and relative humidity increase, creating more favourable conditions for homogeneous and heterogeneous reactions on aerosol surfaces or inside them (Cheng et al., 2016a; Wang et al., 2016; Wu et al., 2018). Such reactions cause rapid formation of secondary aerosol matter and enhanced light extinction during severe winter haze episodes. However, more detailed information on the aerosol and reactive gas chemistry during the aerosol-chemistry-boundary layer feedback and related rapid aerosol mass growth events is still needed (Liu et al., 2019). For instance, it is still unclear which chemical reactions and which compounds in the particulate matter play key

83 roles during such rapid mass growth events.

84

85 The particle number size distribution and chemical composition are considered to be the most

86 important variables influencing the light extinction by aerosol particles. In the atmosphere, the highest

87 contribution to aerosol light extinction comes from organic compounds, nitrate and sulphate in

88 particles with diameters of 100-1000 nm. This is due to the dominant mass fractions of the

89 aforementioned compounds in aerosols that correspond to the peak intensity of solar radiation at

90 wavelengths around 550 nm (Jimenez et al., 2009; Swietlicki et al., 2008). In addition, light scattering

91 which contributes the most to the light extinction by atmospheric aerosols, can be substantially

92 enhanced by the presence of liquid water in the aerosol (Chen et al., 2014; Liu et al., 2019a; Pan et

93 al., 2009; Wang et al.,2020). Hence, quantifying the response of light extinction to different chemical

94 compounds would be helpful in evaluating the feedbacks associated with secondary aerosol

95 production.

96

97 In this study, we focus on the physical and chemical properties of aerosols in Beijing during the winter

98 heating season from October 2018 to February 2019 using state-of-the-art instrumentation. The

99 variation of aerosol chemical composition and the associated light extinction coefficient as a function

100 of the varying mixing layer height are discussed. Our aim is to identify the key chemical components

101 which contribute to the aerosol-chemistry-radiation-boundary layer feedback loop in Beijing.

102

103 **2. Methodology**

104 **2.1. Measurement location and instrumentations**

105 Measurements were conducted between 1 October 2018 and 28 February 2019 at the roof top of the

106 university building at the west campus of Beijing University of Chemical Technology (39.95°N,

107 116.31°E). This station is located about 150 m away from the nearest road (Zizhuyuan road) and 500

108 m away from the West Third Ring Road, and it is surrounded by commercial properties and residential

109   dwellings representative of an urban environment. More details on the location can be found in (Liu

110   et al., 2020; Zhou et al., 2020).

111

112   The meteorological data for this work include basic meteorological variables (relative humidity (RH),

113   temperature, wind speed, wind direction, and visibility) and mixing layer height (MLH) measured

114   using a weather station (Vaisala Inc., Finland) and a Ceilometer CL51 (Vaisala Inc., Finland),

115   respectively. The MLH is defined as the height above the surface, through which relatively vigorous

116   vertical mixing occurs (Holzworth, 1972), and its value is highly related to the vertical temperature

117   structure and, so some extent, to a mechanically-induced turbulence (Baxter, 1991). Here, we

118   followed the method introduced earlier by Münkel et al. (2007) and Eresmaa et al. (2012) in

119   determining the MLH.

120

121   The number size distributions of aerosol particles from 6 nm to 840 nm were measured by a

122   Differential Mobility Particle Sizer (DMPS) (Aalto et al., 2001). The mass concentration of fine

123   particulate matter ($PM_{2.5}$) was measured using a Tapered Element Oscillating Microbalance

124   Dichotomous Ambient Particulate Monitor (TEOM 1405-DF, Thermo Fisher Scientific Inc, USA)

125   with a total flow rate of 16.67 L/min (Wang et al., 2014).

126

127   A time-of-flight aerosol chemical speciation monitor (ToF-ACSM, Aerodyne Research Inc.) was used

128   to measure the concentrations of non-refractory (NR) components, including sulfate, nitrate,

129   ammonium, chloride and organics of $PM_{2.5}$ (Fröhlich et al., 2013). A $PM_{2.5}$ cyclone was deployed on

130   the rooftop with a flow rate of 3 L /min. The correlation coefficient of $PM_{2.5}$ measured by TEOM and

131   ToF-ACSM is around 0.9, which indicates the consistence of the two datasets. Aerosol was dried

132   though a Nafion dryer (MD-700-24F-3, PERMA PURE) before entering the ToF- ACSM. The inlet

133   flow was set at 1.4 cm^3/s. The particle beam passed through the chamber and reached the heated

134   porous tungsten surface (T≈600℃). There, the non-refractory $PM_{2.5}$ constituents were vaporized and

135   then ionized by electrons (E_{kin}=70eV, emitted by a tungsten filament). The ions were measured by a

136   detector and the data was analyzed using Tofware ver. 2.5.13 within IgorPro ver. 6.3.7.2

137 (WaveMetrics). The relative ionization efficiencies (RIE) for sulfate, nitrate, ammonium, chloride

138 and organics applied were 0.86, 1.05, 4.0, 1.5 and 1.4, respectively. Besides RIE correction, the data

139 also did CO_2^+/ NO_3 artifact correction (Pieber et al., 2016) and collection efficiency (CE) correction

140 (Middlebrook et al., 2012). Mass concentrations of ammonium nitrate, ammonium sulfate and

141 ammonium chloride were determined according to the method introduced by Gysel et al. (2007). The

142 aerosol liquid water content (AWC) was calculated by the thermodynamic equilibrium model

143 ISORROPIA II using ToF-ACSM data (Fountoukis and Nenes, 2007).

144 Highly-oxygenated organic molecules (HOMs) were measured by a chemical ionization long time-

145 of-flight mass spectrometer equipped with a nitrate chemical ionization source (LToF-CIMS,

146 Aerodyne Research, Inc. USA) (Jokinen et al., 2012) similar to gas-phase sulfuric acid. The ambient

147 air was drawn into the ionization source through a stainless-steel tube with a length of ~1.6 m and a

148 diameter of 3/4 inch at a flowrate of ~ 8 L/min. A 30-40 L/min purified air flow and a 4-8 mL/min

149 ultrahigh purity nitrogen flow containing nitric acid were mixed together as the sheath flow, which is

150 guided through a PhotoIonizer (Model L9491, Hamamatsu, Japan) to produce nitrate reagent ions.

151 This sheath flow is then introduced into a co-axial laminar flow reactor concentric to the sample flow.

152 Nitrate ions are pushed to the sample flow layer by an electric field and subsequently charge analytical

153 molecules. Organic carbon (OC) and element carbon (EC) concentrations were measured semi-

154 continuously with a 1-hour time resolution using an OC/EC Analyzer (Model-4, Sunset Lab. Inc.)

155 and time series of ACSM Org and Sunset OC as shown in Fig S6.

156 The ammonia is measured by Trace Ammonia analyzer (Los Gatos Research, Inc.) at atmospheric

157 ambient levels with high precision (0.2 ppb in 1s) and ultra-fast response (5 Hz).

158

159 The air mass history was studied by calculating particle retroplumes using a Lagrangian particle

160 dispersion model FLEXPART (FLEXible PARTicle dispersion model) ver. 9.02 (Stohl et al., 2005).

161 The ECMWF (European Centre for Medium-Range Weather Forecast) operational forecast (with 0.15°

162 horizontal and 1 h temporal resolution) was used as the meteorological input into the model. During

163 the measurement period, a new release of 50 000 test particles, distributed evenly between 0 and 100

164 m above the measurement site, occurred every 1 hour. The released particles were traced backwards

165   in time for 72 h, unless they exceeded the model boundary (20–60°N, 95–135°E).

166

167   **2.2. Aerosol light extinction calculation**

168   The aerosol light extinction coefficient was calculated with the Mie-Model, which uses particle

169   number size distribution, mass concentrations of different aerosol compounds and their refractive

170   index as inputs (Seinfeld and Pandis, 2006). We introduced a series of assumptions into the Mie-

171   Model, including 1) "internal mixture" which considers each chemical component in a particle as

172   homogeneously mixed with each other; 2) all particles are spherical; and 3) particles of different sizes

173   have the same chemical composition.

174

175   The practical method introduced under those assumptions in previous studies were found to be

176   capable of estimating a variation trend of optical property of $PM_{0.5-20}$ with a relatively good accuracy

177   (Lin et al., 2013).

178

179   Table 1. Summary of the parameters for calculating the average optical refractive index.

180

Species	ρ_i(g cm^{-3})	n_i	k_i
(NH$_4$)$_2$SO$_4$	1.760	1.530	0.000
NH$_4$NO$_3$	1.725	1.554	0.000
NH$_4$Cl	1.527	1.639	0.000
Organics	1.400	1.550	0.001
EC	1.500	1.800	0.540

181

182   The average optical refractive index (AORI) of an internally-mixed particle can be calculated from

183   the optical refractive indices (ORI) of each chemical component by following a mixing rule of

184   volume-averaged chemical components as AORI = n_{eff} + k_{eff} × i, where the real part (n_{eff}) and

185   imaginary part (k_{eff}) are given by:

$$n_{eff} = \left(\sum_i n_i \cdot m_i/\rho_i \right) \bigg/ \left(\sum_i m_i/\rho_i \right) \qquad (1)$$

$$k_{eff} = \left(\sum_i k_i \cdot m_i/\rho_i \right) \bigg/ \left(\sum_i m_i/\rho_i \right) \qquad (2)$$

186   Here m_i and ρ_i are the mass concentration and density of the component i in particles, respectively,

187   and n_i and k_i are the real and imaginary parts of ORI of this component, respectively. The

188   parameters for calculating the AORI are summarised in Table 1. The values of n_i and k_i in Table 1

189   are referenced to the light wavelength of 550 nm.

190

191   $Q_{sp,j}$ represents light scattering efficiency of a single particle with diameter D_j, while $Q_{ep,j}$

192   represents light absorption efficiency. Theoretically, $Q_{sp,j}$ and $Q_{ep,j}$ are both the function of D_j and

193   the $AORI_j$ (the AORI of the particle with diameter D_j) at a given light wavelength λ, for which the

194   complicated calculations were referenced to a previous publication (Lin et al., 2013). Regarding the

195   limitations of measurement techniques, the $AORI_j$ was assumed to be equal to the $AORI_{PM2.5}$, which

196   was determined based on chemical composition of $PM_{2.5}$. It is possible to derive expressions for the

197   cross sections of a spherical particle exactly. The formulas for $Q_{sp,j}$ and $Q_{ep,j}$ are:

198

$$Q_{sp,j}(D_j, \lambda, AORI_j) = \frac{2}{\alpha^2} \sum_{k=1}^{\infty} (2k+1) \cdot [|a_k|^2 + |b_k|^2] \qquad (3)$$

$$Q_{ep,j}(D_j, \lambda, AORI_j) = \frac{2}{\alpha^2} \sum_{k=1}^{\infty} (2k+1) \cdot Re[a_k + b_k] \qquad (4)$$

199

200   where

201

$$a_k = \frac{\alpha\psi_k'(y)\psi_k(\alpha) - y\psi_k'(\alpha)\psi_k(y)}{\alpha\psi_k'(y)\xi_k(\alpha) - y\xi_k'(\alpha)\psi_k(y)}$$

203

$$b_k = \frac{y\psi_k'(y)\psi_k(\alpha) - \alpha\psi_k'(\alpha)\psi_k(y)}{y\psi_k'(y)\xi_k(\alpha) - \alpha\xi_k'(\alpha)\psi_k(y)}$$

205

206   with $y = \alpha m$.

207

$$m = n_{eff} + i \cdot k_{eff}$$

208

209

$$\alpha = \frac{\pi D_j}{\lambda}$$

210

211

212   with λ = 550 nm.

213

214   where complex number m stands for $AORI_j$, while α is the size of the particle, usually expressed as

215   a dimensionless size parameter. The functions $\psi_k(z)$ and $\xi_k(z)$ are the Riccati–Bessel functions:

$$\psi_k(z) = \left(\frac{\pi z}{2}\right)^{1/2} J_{k+1/2}(z) \tag{5}$$

$$\xi_k(z) = \left(\frac{\pi z}{2}\right)^{1/2} \left[J_{k+1/2}(z) + i(-1)^k J_{-k-1/2}(z)\right] \tag{6}$$

216

217   where $J_{k+1/2}$ and $J_{-k-1/2}$ are the Bessel functions of the first kind and their footnotes indicate the

218   order of Bessel functions. The Mie theory can serve as the basis of a computational procedure to

219   calculate the scattering and absorption of light by any sphere as a function of wavelength.

220

221   According to the Mie-Model, b_{sp} (light scattering coefficient) and b_{ep} (light extinction coefficient)

222   can be quantified with Eqs. (5) and (6), respectively. b_{ap} (light absorption coefficient) is the

223   difference between b_{ep} and b_{sp}, which equals zero, when k_i equals zero or very small. Optical

224   properties including b_{ep}, b_{sp} and b_{ap} to be discussed later are all referenced to light wavelength of

225   550 nm.

$$b_{sp} = \sum_j b_{sp,j} = \sum_j \frac{\pi D_j^2}{4} \cdot Q_{sp,j}(D_j, \lambda, AORI_j) \cdot N_j \tag{7}$$

$$b_{ep} = \sum_j b_{ep,j} = \sum_j \frac{\pi D_j^2}{4} \cdot Q_{ep,j}(D_j, \lambda, AORI_j) \cdot N_j \tag{8}$$

226

227

228   In Eqs. (7) and (8), D_j stands for the median Stokes diameter in the j-th particle size range and N_j is

229   the number concentration of particles with diameter, D_j.

230

231   **3. Results and discussion**

3.1. An over of the measurement campaign

The time series particle number size distribution from 6 nm to 840 nm, mass concentrations of nitrate, organics, sulfate, ammonium and chloride in NR_PM$_{2.5}$ (non-refractory PM$_{2.5}$) and PM$_{2.5}$, concentration of HOMs and OC are shown in Figure 1(a), (b) and (c). The statistics of these compounds are summarized in Table S1. In general, they showed similar variation patterns (Figure S2 and S3). These concentrations showed high values during haze event than clean days and increased significantly during night time. As shown in Figure 1(b), the rapid mass growth during the heating season in Beijing is related to the rapid growth in nitrate concentration. At the same time, the haze events (PM$_{2.5}$ concentration >= 75μg/m^3 and lasting more than one day) are accompanied by particle size growth (Figure 1(a)). To further study which particle size possesses the highest light extinction efficiency during the haze events, and to what extent nitrates contribute to light extinction with the variation of MLH, a case of rapid rapid aerosol mass growth event is selected for further study.

232   **3.2. Typical case of rapid aerosol mass growth episodes affected by aerosol-chemistry-**
233   **boundary layer interactions**

234   An example of rapid aerosol mass growth in urban wintertime Beijing is illustrated in Figure 2, where

235   the haze accumulation was associated with a rapid PM$_{2.5}$ mass concentration increase from 8.5 μg/m^3

236   to more than 100 μg/m^3 in less than 7 hours. A haze episode started on afternoon 20 February 2019

237   under stagnant meteorological conditions with low wind speeds and elevated ambient relative

238   humidity (Figure S4). The polluted periods during this case occurred under southerly wind transport

239   conditions, whereas clean air masses originated from the north-westerly regions (as shown in Figure

240   S5, S6). These are typical features for a haze evolution process in Beijing (Wang et al., 2020b). During

241   the haze periods marked by the shaded areas in Figure 2, an obvious increase of chemical mass

242   concentration was observed by the ToF-ACSM, characterised by high concentrations of secondary

243   aerosol components (nitrate, organics and sulphate) and typically a shallow boundary layer. The mass

244   concentrations of organics, sulphate and nitrate increased dramatically with a decreasing MLH,

245   accounting for 88.5% of NR-PM$_{2.5}$ during the rapid aerosol mass growth period. The aerosol mass

246   growth was the fastest for nitrate. The mass concentrations of organic and elemental carbon followed

247   that of NR-PM$_{2.5}$.

248

249   The MLH reached its maximum at around 14:00 in the afternoon of 20 February, after which the

250   development of the mixing layer was suppressed and MLH decreased with the arrival of pollution

251   (Figure 2a). Previous studies have shown that the aerosol-radiation-boundary layer feedback

252   contributes to a rapid enhancement of air pollution (Petäjä et al., 2016; Wang et al., 2020d). High

253   concentrations of aerosol particles obscure downward radiation, as a result of which the surface

254   temperature and sensitive heat flux decrease and the development of mixing layer height is suppressed.

255   Recent studies have gradually realized that the facilitation of various chemical processes play a non-

256   negligible role in the aerosol-radiation-boundary layer feedback (Liu.Q et al., 2018; Liu. Z et al.,2019).

257   Therefore, it is important to identify and quantify the role of different specific chemical species and

258   particle size ranges in reducing atmospheric radiation and extinction.

259

260   Figure 3 shows the contributions of size and chemical composition-resolved dry aerosol to light

261   extinction during the investigated period. As the pollution intensified and MLH decreased (Fig 2c),

262   the light extinction of atmospheric aerosols increased significantly. Assuming that particles of

263   different sizes have the same chemical composition as PM$_{2.5}$ (organics, NH$_4$NO$_3$, EC, (NH$_4$)$_2$SO$_4$,

264   NH$_4$Cl), the light extinction of particles in the size range of 300-700 nm increased significantly from

265   the relative clean period to the polluted period (namely from 12:00 to 16:00). During relatively clean

266   conditions, the contributions of organics, NH$_4$NO$_3$, EC, (NH$_4$)$_2$SO$_4$ and NH$_4$Cl to the total aerosol

267   light extinction were 42%, 23%, 18%, 11% and 7%, respectively. The contribution of NH$_4$NO$_3$ to

268   aerosol light extinction reached 40% during the heavily polluted period. Based on the observation it

269   is likely that the increased light extinction by aerosols reduced solar radiation reaching the surface,

270   so that the development of the boundary layer was suppressed.

271

**3.3. Connection between the aerosol chemical composition, light extinction, size distribution
       and MLH during the heating season**

274

275   To better characterize the effect of the chemical composition of dry aerosols and the PNSD (particle

276   number size distribution) light extinction under different MLH conditions, the daytime (8:00 – 16:00

277   LT) measurement data from October 2018 to February 2019 were selected for further analysis. As

278   shown by Figure 4 and consistent with other observations in Beijing (Tang et al., 2016; Wang et al.,

279   2020c), there was a general tendency for the $PM_{2.5}$ mass concentration to increase with a decreasing

280   MLH. Organic compounds and nitrate were the most abundant fractions of the daytime aerosol mass

281   composition, contributing together approximately 70% to total NR-$PM_{2.5}$ mass concentration. With a

282   decreasing MLH, the fraction of nitrate mass in NR-$PM_{2.5}$ slightly increased while that of organics

283   decreased. This feature makes the aerosol more hygroscopic under low MLH conditions typical for

284   heavily polluted periods. The increased nitrate fraction in the aerosol could also enhance the

285   formation of other secondary aerosol components (Xue et al., 2019). Note that some fraction of

286   aerosol nitrate could consist of organic nitrate originating from reaction of peroxy radical with nitric

287   oxide; however, it is difficult to distinguish organic nitrate from inorganic nitrate at the moment due

288   to instrumental limitations (Fröhlich et al., 2013).

289

290   Figure 5 depicts the calculated daytime light extinction of the dry aerosol as a function of the MLH,

291   separated by different size ranges and chemical components. We may see that in general, particles

292   with dry diameters in the range of 300-700 nm explains more than 80% of the total aerosol light

293   extinction (Figure 5b). Similar to their share in NR-$PM_{2.5}$, the fraction of light extinction by

294   ammonium nitrate increased and that of organics decreased during the lowest MLH conditions

295 corresponding to the heavy pollution periods (Figure 5d). There are also apparent differences in the

296 relative contribution of different particle size ranges to light extinction in different MLH conditions:

297 with a decreasing MLH, the contribution of particles with dry dimeters larger than about 400-500 nm

298 clearly increased while that of sub-300 nm particles notably decreased. This indicates that the

299 enhanced light extinction by the dry aerosol at low MLH conditions was not only due the more

300 abundant aerosol mass concentration, but also due to the growth of individual particles to optically

301 more active sizes.

302

303 At relative humidity larger than about 70%, aerosol liquid water gives a significant contribution to

304 the aerosol mass concentration and often a dominant contribution to the aerosol light extinction (Titos

305 et al., 2016). This has important implications for the aerosol-chemistry-radiation-boundary layer

306 feedback, when considering our findings listed above and further noting that heavy pollution periods

307 are often accompanied by high values of RH in Beijing (Zhong et al., 2018). First, compared to clean

308 or moderately-polluted conditions, the enhancement in the aerosol light extinction under polluted is

309 probably much larger than that illustrated in Figure 5. Second, the high aerosol water content under

310 polluted conditions promotes many kinds of chemical reactions taking place on the surface or inside

311 aerosol particles.

312

3.4. Aerosol-chemistry-radiation-boundary layer interaction

314

315 In order to further investigate the interaction between MLH and chemical compounds (either observed

316 or calculated), we divided the observed $PM_{2.5}$ concentrations into highly polluted and less polluted

317 conditions using a threshold value of 75 μg /m^3 for $PM_{2.5}$. The organics, nitrate, ammonium, sulfate,

318 chloride, HOM, aerosol water content (AWC) and $PM_{2.5}$ as a function of the mixing layer height

319 during both highly polluted and less polluted conditions are shown in Figure 6. The fitted relationships

320 connecting the concentrations of different chemical compounds to the reduction of MLH under highly

321 and less polluted conditions allowed us to estimate the net mass concentration increase of each

322   compound due to secondary formation and aerosol-chemical-boundary layer feedback under highly

323   polluted conditions (shaded areas in Figure 6). It is worth noting that AWC, nitrate and sulfate

324   increased the most as the MLH decreased, as represented by the large shaded areas in Figs. 6 (h), (b)

325   and (c). The increases of these components are significant as tested (Supplement information). The

326   day-time nitrate in aerosol is formed predominately via the reaction of nitric acid and ammonium,

327   while nitric acid is produced from gas phase reaction of nitrogen dioxide and hydroxy radical

328   (Seinfeld and Pandis, 2006). High concentrations of daytime nitrate aerosols indicate efficient

329   production of gas phase nitric acid, its partitioning into liquid aerosol and its fast neutralization by

330   abundant ammonia (Li et al., 2018a; Pan et al., 2016; Wang et al., 2020). A recent study shows that

331   condensation of nitric acid and ammonia could promote fast growth of newly formed particle in urban

332   environment condition (Wang et al., 2020d). Another possibility is that ammonium nitrate is formed

333   rapidly on particle surfaces due to the hydrolysis of dinitrogen pentoxide (N_2O_5) during daytime, as

334   the AWC increased significantly (Wang et al., 2014;Wang et al.,2020). However, a quantitative

335   distinction between the two formation pathways for nitrate formation is not possible in this study. The

336   dramatic increase of nitrate aerosol could also promote the formation of sulfate by heterogeneous

337   reactions (Cheng et al., 2016b; Wang et al., 2016). The concentration of HOMs showed a slight

338   increase as the MLH decreased, which suggests that also the formation of HOMs is enhanced with an

339   increased level of air pollution. This phenomenon should be further investigated as HOMs can

340   substantially contribute to the secondary organic aerosol formation.

341

342   Figure 7 displays the dry aerosol light extinction by different chemical compounds in the same way

343   as Figure 6 did for aerosol mass concentrations. The aerosol light extinction is directly related to the

344   reduction of solar radiation reaching the surface, assuming that aerosol chemical components are

345   vertically nearly homogeneously distributed. The light extinction from ammonium nitrate,

346   ammonium sulfate and organics showed significantly increased contributions under highly polluted

347   conditions (low MLH) as compared with less polluted conditions. To the contrary, no such

348   enhancement was observed for ammonium chloride or element carbon (Figs. 7 (d) and (e)). In case

349   of EC this is an expected result, as it originates solely from primary sources. The formation of particle

phase chloride have secondary sources from chlorine atom-initiated oxidation of volatile organic compounds, so that the resulting oxidation products could contribute to the observed chloride (Wang and Ruiz, 2017; Wang et al., 2019a).

To better illustrate the combined effects of secondary aerosol formation and associated feedback on the daytime mass concentrations and light extinction due to different chemical components, we scaled these quantities by either the total $PM_{2.5}$ mass concentration or EC concentration and plotted them as a function of MLH (Fig. 8). With the average level of $PM_{2.5}$ measured by TEOM and ToF-ACSM, the latter scaling minimizes the boundary layer accumulation effect on our analysis, as EC originates from primary emission sources (Cao et al., 2006). As shown in Fig. 8a, organics with their mass fraction of 61% were the most abundant component in $PM_{2.5}$ under high MLH conditions, followed by nitrate and ammonium with their mass fractions of 22% and 13%, respectively. The aerosol was estimated to be rather dry under high MLH conditions ($AWC/PM_{2.5} = 0.03$). However, with the decreasing MLH, the fraction of nitrate and the AWC to $PM_{2.5}$ ratio increased up to 45% and 0.2, respectively. This clearly indicates rapid nitrate formation and dramatic increase of the aerosol water uptake from less polluted conditions to intensive haze pollution. Compared with EC (Fig.8c), the concentrations of organic compounds, nitrate, sulfate and ammonium increased by factors of 1.5, 6.3, 4.8 and 4.9 respectively, from the highest to the lowest MLH conditions. Thus, although organics remained as the second most abundant aerosol component after nitrate under haze conditions, secondary formation and associated feedback from less to highly polluted conditions were clearly stronger for both sulfate and ammonium. Efficient sulfate production associated with haze formation has been reported in several studies conducted in China (Cheng et al., 2016; Xie et al., 2015; Xue et al., 2016). Ammonium production during haze formation is tied with neutralization of acidic aerosol by ammonia, which was apparently present abundantly in the gas phase. Compared with the EC concentration, light extinction by (NH_4NO_3) increased the most from the highest MLH conditions ($248 \text{ M m}^{-1}/\mu\text{g m}^{-3}$) to the lowest MLH conditions ($1150 \text{ M m}^{-1}/\mu\text{g m}^{-3}$) as shown by Figure 8b. Overall, the rapid growth of nitrate aerosol mass, together with abundant concentration of organic aerosol, were the main cause of the light extinction for dry aerosol under haze formation.

378

The mechanism governing the aerosol-chemistry-radiation-boundary layer feedback for the rapid growth of atmospheric aerosol is illustrated in Fig. 9. As a result of reduction in solar radiation and atmospheric heating, a variety of chemical reactions in the gas phase and on particle surfaces or inside them are enhanced with an increased relative humidity and AWC. Such conditions are unfavorable for the dispersion of pollutants, which further enhances atmospheric stability. The formation of hydrophilic compounds, e.g., nitrate, sulfate and oxygenated organic compounds, result in enhanced water uptake by aerosol particles, which will essentially increase heterogeneous reactions associated with these particles. As a result, the aerosol mass and size increase, light extinction is enhanced, and the development of the mixing layer is depressed. At the same time, aerosol precursors concentrated within a shallower mixing layer lead to enhanced production rate of aerosol components in both gas and aerosol phases, especially nitrate but also other secondary aerosol. The increased concentrations of aerosol will further enhance this positive loop.

4. Conclusions

We investigated the synergetic variations of aerosol chemical composition and mixing layer height during the daytime in urban Beijing. Significant dependency of the sharp increase of ammonium nitrate and aerosol water content with the occurrence of the explosive aerosol mass growth events were observed. We showed that these two components drove a positive aerosol-chemistry-radiation-boundary layer feedback loop, which played an important role in the explosive aerosol mass growth events. A plausible explanation is that the increased aerosol water content at low mixing layer heights provides favorable conditions for heterogeneous reactions for nitrate and sulfate production and neutralization by ammonia. The significant formation of secondary aerosol increases the concentration of aerosol particles in the diameter range 300-700 nm, which effectively reduces the solar radiation reaching the surface and further enhances the aerosol-chemistry-radiation-boundary layer feedback loop. Our analysis connects the aerosol light extinction to a reduction in the mixing

layer height, which suppresses the volume into which air pollutants are emitted and leads to an explosive aerosol mass growth. Our results indicate that reduction of ammonium and nitrate concentration in aerosol could weaken the aerosol-radiation-chemistry-boundary layer feedback loop, which could thereby reduce heavy haze episodes in Beijing.

5. Acknowledgements

This work was supported by the funding from Beijing University of Chemical Technology. The European Research Council via advanced grant ATM-GTP (project no. 742206) and Academy of Finland via Academy professor project of M. K.

6. Competing financial interests

The authors declare no competing financial interests.

7. Author contributions

YW and MK initiated the study. ZL, YW, FZ, YZ, YG, ZF, CL, YZ, TC, CY, KD, BC, JK, LY, XF, WD, JC and YL conducted the longtime measurements. ZL, YW, LD, RC, SH, PZ, LW, VK, YL and MK interpreted the data. ZL, YW and VK wrote the manuscript.

422 **Reference**

Aalto, P., Hämeri, K., Becker, E. D. O., Weber, R., Salm, J., Mäkelä, J. M., Hoell, C., O'Dowd, C. D., Karlsson, H., Hansson, H., Väkevä, M., Koponen, I. K., Buzorius, G. and Kulmala, M.: Physical characterization of aerosol particles during nucleation events, Tellus, Series B: Chemical and Physical Meteorology, 53(4), 344–358, doi:10.3402/tellusb.v53i4.17127, 2001.

An, Z., Huang, R.-J., Zhang, R., Tie, X., Li, G., Cao, J., Zhou, W., Shi, Z., Han, Y., Gu, Z. and Ji, Y.: Severe haze in northern China: A synergy of anthropogenic emissions and atmospheric processes, Proceedings of the National Academy of Sciences, 116(18), 8657 LP – 8666, doi:10.1073/pnas.1900125116, 2019.

Baxter, R.: Determination of mixing heights from data collected during the 1985 SCCCAMP field program, Journal of Applied Meteorology, 30(5), 598–606, doi:10.1175/1520-0450(1991)030<0598:DOMHFD>2.0.CO;2, 1991.

Cao, G., Zhang, X. and Zheng, F.: Inventory of black carbon and organic carbon emissions from China, Atmospheric Environment, 40(34), 6516–6527, doi:10.1016/j.atmosenv.2006.05.070, 2006.

Che, H., Zhang, X., Li, Y., Zhou, Z. and Qu, J. J.: Horizontal visibility trends in China 1981-2005, Geophysical Research Letters, 34(24), doi:10.1029/2007GL031450, 2007.

Chen, J., Zhao, C. S., Ma, N. and Yan, P.: Aerosol hygroscopicity parameter derived from the light scattering enhancement factor measurements in the North China Plain, Atmos. Chem. Phys, 14, 8105–8118, doi:10.5194/acp-14-8105-2014, 2014.

Cheng, Y., Zheng, G., Wei, C., Mu, Q., Zheng, B., Wang, Z., Gao, M., Zhang, Q., He, K., Carmichael, G., Pöschl, U. and Su, H.: Reactive nitrogen chemistry in aerosol water as a source of sulfate during haze events in China, Science Advances, 2(12), e1601530–e1601530, doi:10.1126/sciadv.1601530, 2016b.

Ding, A. J., Huang, X., Nie, W., Sun, J. N., Kerminen, V. M., Petäjä, T., Su, H., Cheng, Y. F., Yang, X. Q., Wang, M. H., Chi, X. G., Wang, J. P., Virkkula, A., Guo, W. D., Yuan, J., Wang, S. Y., Zhang, R. J., Wu, Y. F., Song, Y., Zhu, T., Zilitinkevich, S., Kulmala, M. and Fu, C. B.: Enhanced haze pollution by black carbon in megacities in China, Geophysical Research Letters, 43(6), 2873–2879, doi:10.1002/2016GL067745, 2016.

Eresmaa, N., Härkönen, J., Joffre, S. M., Schultz, D. M., Karppinen, A. and Kukkonen, J.: A Three-Step Method for Estimating the Mixing Height Using Ceilometer Data from the Helsinki Testbed, Journal of Applied Meteorology and Climatology, 51(12), 2172–2187, doi:10.1175/JAMC-D-12-058.1, 2012.

Fountoukis, C. and Nenes, A.: ISORROPIA II: a computationally efficient thermodynamic equilibrium model for $K^+–Ca^{2+}–Mg^{2+}–NH_4^+–Na^+–SO_4^{2-}–NO_3^-$, Atmospheric Chemistry and Physics, 7(17), 4639–4659, doi:10.5194/acp-7-4639-2007, 2007.

Fröhlich, R., Cubison, M. J., Slowik, J. G., Bukowiecki, N., Prévôt, A. S. H., Baltensperger, U., Schneider, J., Kimmel, J. R., Gonin, M., Rohner, U., Worsnop, D. R. and Jayne, J. T.: The ToF-ACSM: A portable aerosol chemical speciation monitor with TOFMS detection, Atmospheric Measurement Techniques, 6(11), 3225–3241, doi:10.5194/amt-6-3225-2013, 2013.

Gysel, M., Crosier, J., Topping, D. O., Whitehead, J. D., Bower, K. N., Cubison, M. J., Williams, P. I., Flynn, M. J., McFiggans, G. B. and Coe, H.: Closure study between chemical composition and hygroscopic growth of aerosol particles during TORCH2, Atmospheric Chemistry and Physics, 7(24), 6131–6144, doi:10.5194/acp-7-6131-2007, 2007.

Holzworth, G. C.: Mixing heights, wind speeds, and potential for urban air pollution throughout the contiguous united states, , 118, 1972.

Jimenez, J. L., Canagaratna, M. R., Donahue, N. M., Prevot, A. S. H., Zhang, Q., Kroll, J. H., DeCarlo, P. F., Allan, J. D., Coe, H., Ng, N. L., Aiken, A. C., Docherty, K. S., Ulbrich, I. M., Grieshop, A. P., Robinson, A. L., Duplissy, J., Smith, J. D., Wilson, K. R., Lanz, V. A., Hueglin, C., Sun, Y. L., Tian, J., Laaksonen, A., Raatikainen, T., Rautiainen, J., Vaattovaara, P., Ehn, M., Kulmala, M., Tomlinson, J. M., Collins, D. R., Cubison, M. J., Dunlea, E. J., Huffman, J. A., Onasch, T. B., Alfarra, M. R., Williams, P. I., Bower, K., Kondo, Y., Schneider, J., Drewnick, F., Borrmann, S., Weimer, S., Demerjian, K., Salcedo, D., Cottrell, L., Griffin, R., Takami, A., Miyoshi, T., Hatakeyama, S., Shimono, A., Sun, J. Y., Zhang, Y. M., Dzepina, K., Kimmel, J. R., Sueper, D., Jayne, J. T., Herndon, S. C., Trimborn, A. M., Williams, L. R., Wood, E. C., Middlebrook, A. M., Kolb, C. E., Baltensperger, U. and Worsnop, D. R.: Evolution of organic

aerosols in the atmosphere, Science, 326(5959), 1525–1529, doi:10.1126/science.1180353, 2009.

Jokinen, T., Sipilä, M., Junninen, H., Ehn, M., Lönn, G., Hakala, J., Petäjä, T., Mauldin, R. L., Kulmala, M. and Worsnop, D. R.: Atmospheric sulphuric acid and neutral cluster measurements using CI-APi-TOF, Atmospheric Chemistry and Physics, 12(9), 4117–4125, doi:10.5194/acp-12-4117-2012, 2012.

Lelieveld, J., Evans, J. S., Fnais, M., Giannadaki, D. and Pozzer, A.: The contribution of outdoor air pollution sources to premature mortality on a global scale, Nature, 525(7569), 367–371, doi:10.1038/nature15371, 2015.

Li, H., Zhang, Q., Zheng, B., Chen, C., Wu, N., Guo, H., Zhang, Y., Zheng, Y., Li, X. and He, K.: Nitrate-driven urban haze pollution during summertime over the North China Plain, Atmospheric Chemistry and Physics, 18(8), 5293–5306, doi:10.5194/acp-18-5293-2018, 2018a.

Li, J., Sun, J., Zhou, M., Cheng, Z., Li, Q., Cao, X. and Zhang, J.: Observational analyses of dramatic developments of a severe air pollution event in the Beijing area, Atmospheric Chemistry and Physics, 18(6), 3919–3935, doi:10.5194/acp-18-3919-2018, 2018b.

Lin, Z. J., Tao, J., Chai, F. H., Fan, S. J., Yue, J. H., Zhu, L. H., Ho, K. F. and Zhang, R. J.: Impact of relative humidity and particles number size distribution on aerosol light extinction in the urban area of Guangzhou, Atmospheric Chemistry and Physics, 13(3), 1115–1128, doi:10.5194/acp-13-1115-2013, 2013.

Liu, G., Xin, J., Wang, X., Si, R., Ma, Y., Wen, T., Zhao, L., Zhao, D., Wang, Y. and Gao, W.: Impact of the coal banning zone on visibility in the Beijing-Tianjin-Hebei region, Science of the Total Environment, 692, 402–410, doi:10.1016/j.scitotenv.2019.07.006, 2019a.

Liu, Q., Jia, X., Quan, J., Li, J., Li, X., Wu, Y., Chen, D., Wang, Z. and Liu, Y.: New positive feedback mechanism between boundary layer meteorology and secondary aerosol formation during severe haze events, Scientific Reports, 8(1), doi:10.1038/s41598-018-24366-3, 2018.

Liu, Y., Zhang, Y., Lian, C., Yan, C. and Feng, Z.: The promotion effect of nitrous acid on aerosol formation in wintertime Beijing : possible contribution of traffic-related emission, Atmos. Chem. Phys. Discuss., 2020(February), 1–43, doi:10.5194/acp-2020-150, 2020.

Liu, Z., Hu, B., Ji, D., Cheng, M., Gao, W., Shi, S., Xie, Y., Yang, S., Gao, M., Fu, H., Chen, J. and

Wang, Y.: Characteristics of fine particle explosive growth events in Beijing, China: Seasonal variation, chemical evolution pattern and formation mechanism, Science of the Total Environment, 687, 1073–1086, doi:10.1016/j.scitotenv.2019.06.068, 2019b.

Münkel, C., Eresmaa, N., Räsänen, J. and Karppinen, A.: Retrieval of mixing height and dust concentration with lidar ceilometer, Boundary-Layer Meteorology, 124(1), 117–128, doi:10.1007/s10546-006-9103-3, 2007.

Pan, X. L., Yan, P., Tang, J., Ma, J. Z., Wang, Z. F., Gbaguidi, A. and Sun, Y. L.: Observational study of influence of aerosol hygroscopic growth on scattering coefficient over rural area near Beijing mega-city, Atmospheric Chemistry and Physics, 9(19), 7519–7530, doi:10.5194/acp-9-7519-2009, 2009.

Pan, Y., Tian, S., Liu, D., Fang, Y., Zhu, X., Zhang, Q., Zheng, B., Michalski, G. and Wang, Y.: Fossil Fuel Combustion-Related Emissions Dominate Atmospheric Ammonia Sources during Severe Haze Episodes: Evidence from 15N-Stable Isotope in Size-Resolved Aerosol Ammonium, Environmental Science and Technology, 50(15), 8049–8056, doi:10.1021/acs.est.6b00634, 2016.

Petäjä, T., Järvi, L., Kerminen, V. M., Ding, A. J., Sun, J. N., Nie, W., Kujansuu, J., Virkkula, A., Yang, X., Fu, C. B., Zilitinkevich, S. and Kulmala, M.: Enhanced air pollution via aerosol-boundary layer feedback in China, Scientific Reports, 6, doi:10.1038/srep18998, 2016.

Pieber, S. M., El Haddad, I., Slowik, J. G., Canagaratna, M. R., Jayne, J. T., Platt, S. M., Bozzetti, C., Daellenbach, K. R., Fröhlich, R., Vlachou, A., Klein, F., Dommen, J., Miljevic, B., Jiménez, J. L., Worsnop, D. R., Baltensperger, U. and Prévôt, A. S. H.: Inorganic Salt Interference on CO2+ in Aerodyne AMS and ACSM Organic Aerosol Composition Studies, Environmental Science and Technology, 50(19), 10494–10503, doi:10.1021/acs.est.6b01035, 2016.

Spracklen, D. V., Carslaw, K. S., Kulmala, M., Kerminen, V. M., Sihto, S. L., Riipinen, I., Merikanto, J., Mann, G. W., Chipperfield, M. P., Wiedensohler, A., Birmili, W. and Lihavainen, H.: Contribution of particle formation to global cloud condensation nuclei concentrations, Geophysical Research Letters, 35(6), doi:10.1029/2007GL033038, 2008.

Stohl, A., Forster, C., Frank, A., Seibert, P. and Wotawa, G.: Technical note: The Lagrangian particle dispersion model FLEXPART version 6.2, Atmospheric Chemistry and Physics, 5(9),

2461–2474, doi:10.5194/acp-5-2461-2005, 2005.

Swietlicki, E., Hansson, H.-C., Hämeri, K., Svenningsson, B., Massling, A., Mcfiggans, G., Mcmurry, P. H., Petäjä, T., Tunved, P., Gysel, M., Topping, D., Weingartner, E., Baltensperger, U., Rissler, J., Wiedensohler, A. and Kulmala, M.: Hygroscopic properties of submicrometer atmospheric aerosol particles measured with H-TDMA instruments in various environments—a review, Tellus B: Chemical and Physical Meteorology, 60(3), 432–469, doi:10.1111/j.1600-0889.2008.00350.x, 2008.

Tang, G., Zhang, J., Zhu, X., Song, T., Münkel, C., Hu, B., Schäfer, K., Liu, Z., Zhang, J., Wang, L., Xin, J., Suppan, P. and Wang, Y.: Mixing layer height and its implications for air pollution over Beijing, China, Atmos. Chem. Phys, 16, 2459–2475, doi:10.5194/acp-16-2459-2016, 2016.

Titos, G., Cazorla, A., Zieger, P., Andrews, E., Lyamani, H., Granados-Muñoz, M. J., Olmo, F. J. and Alados-Arboledas, L.: Effect of hygroscopic growth on the aerosol light-scattering coefficient: A review of measurements, techniques and error sources, Atmospheric Environment, 141, 494–507, doi:10.1016/j.atmosenv.2016.07.021, 2016.

Vanhanen, J., Mikkilä, J., Lehtipalo, K., Sipilä, M., Manninen, H. E., Siivola, E., Petäjä, T. and Kulmala, M.: Particle size magnifier for nano-CN detection, Aerosol Science and Technology, 45(4), 533–542, doi:10.1080/02786826.2010.547889, 2011.

Wang, G., Zhang, R., Gomez, M. E., Yang, L., Zamora, M. L., Hu, M., Lin, Y., Peng, J., Guo, S., Meng, J., Li, J., Cheng, C., Hu, T., Ren, Y., Wang, Y., Gao, J., Cao, J., An, Z., Zhou, W., Li, G., Wang, J., Tian, P., Marrero-Ortiz, W., Secrest, J., Du, Z., Zheng, J., Shang, D., Zeng, L., Shao, M., Wang, W., Huang, Y., Wang, Y., Zhu, Y., Li, Y., Hu, J., Pan, B., Cai, L., Cheng, Y., Ji, Y., Zhang, F., Rosenfeld, D., Liss, P. S., Duce, R. A., Kolb, C. E. and Molina, M. J.: Persistent sulfate formation from London Fog to Chinese haze, Proceedings of the National Academy of Sciences of the United States of America, 113(48), 13630–13635, doi:10.1073/pnas.1616540113, 2016.

Wang, H., Peng, Y., Zhang, X., Liu, H., Zhang, M., Che, H. and Cheng, Y.: Contributions to the explosive growth of PM 2 . 5 mass due to aerosol – radiation feedback and decrease in turbulent diffusion during a red alert heavy haze in Beijing – Tianjin – Hebei , China, , 17717–17733, 2018a.

Wang, J., Wang, S., Jiang, J., Ding, A., Zheng, M., Zhao, B., Wong, D. C., Zhou, W., Zheng, G.,

Wang, L., Pleim, J. E. and Hao, J.: Impact of aerosol-meteorology interactions on fine particle pollution during China's severe haze episode in January 2013, Environmental Research Letters, 9(9), doi:10.1088/1748-9326/9/9/094002, 2014a.

Wang, M., Kong, W., Marten, R., He, X.-C., Chen, D., Pfeifer, J., Heitto, A., Kontkanen, J., Dada, L., Kürten, A., Yli-Juuti, T., Manninen, H. E., Amanatidis, S., Amorim, A., Baalbaki, R., Baccarini, A., Bell, D. M., Bertozzi, B., Bräkling, S., Brilke, S., Murillo, L. C., Chiu, R., Chu, B., De Menezes, L.-P., Duplissy, J., Finkenzeller, H., Carracedo, L. G., Granzin, M., Guida, R., Hansel, A., Hofbauer, V., Krechmer, J., Lehtipalo, K., Lamkaddam, H., Lampimäki, M., Lee, C. P., Makhmutov, V., Marie, G., Mathot, S., Mauldin, R. L., Mentler, B., Müller, T., Onnela, A., Partoll, E., Petäjä, T., Philippov, M., Pospisilova, V., Ranjithkumar, A., Rissanen, M., Rörup, B., Scholz, W., Shen, J., Simon, M., Sipilä, M., Steiner, G., Stolzenburg, D., Tham, Y. J., Tomé, A., Wagner, A. C., Wang, D. S., Wang, Y., Weber, S. K., Winkler, P. M., Wlasits, P. J., Wu, Y., Xiao, M., Ye, Q., Zauner-Wieczorek, M., Zhou, X., Volkamer, R., Riipinen, I., Dommen, J., Curtius, J., Baltensperger, U., Kulmala, M., Worsnop, D. R., Kirkby, J., Seinfeld, J. H., El-Haddad, I., Flagan, R. C. and Donahue, N. M.: Rapid growth of new atmospheric particles by nitric acid and ammonia condensation, Nature, 581(7807), 184–189, doi:10.1038/s41586-020-2270-4, 2020d.

Wang, X., Wang, T., Yan, C., Tham, Y. J., Xue, L., Xu, Z. and Zha, Q.: Large daytime signals of N2O5 and NO3 inferred at 62 amu in a TD-CIMS: Chemical interference or a real atmospheric phenomenon, Atmospheric Measurement Techniques, 7(1), 1–12, doi:10.5194/amt-7-1-2014, 2014b.

Wang, Y., Riva, M., Xie, H. and Heikkinen, L.: Formation of highly oxygenated organic molecules from chlorine atom initiated oxidation of alpha-pinene, Atmospheric Chemistry and Physics, 2020, 1–31, doi:10.5194/acp-2019-807, 2020.

Wang, Y., Wang, Y., Wang, L., Petäjä, T., Zha, Q., Gong, C., Li, S., Pan, Y., Hu, B., Xin, J. and Kulmala, M.: Increased inorganic aerosol fraction contributes to air pollution and haze in China, Atmos. Chem. Phys, 19, 5881–5888, doi:10.5194/acp-19-5881-2019, 2019b.

Wang, Y., Gao, W., Wang, S., Song, T., Gong, Z., Ji, D., Wang, L., Liu, Z., Tang, G., Huo, Y., Tian, S., Li, J., Li, M., Yang, Y., Chu, B., Petäjä, T., Kerminen, V.-M., He, H., Hao, J., Kulmala,

M., Wang, Y. and Zhang, Y.: Contrasting trends of PM2.5 and surface ozone concentrations in China from 2013 to 2017, National Science Review, doi:10.1093/nsr/nwaa032, 2020b.

Wang, Y., Chen, Y., Wu, Z., Shang, D., Bian, Y., Du, Z. and Schmitt, S. H.: Mutual promotion between aerosol particle liquid water and particulate nitrate enhancement leads to severe nitrate-dominated particulate matter pollution and low visibility, Atmos. Chem. Phys, (September 2020), 2161–2175, 2020c.

Wang, Y., Yu, M., Wang, Y., Tang, G., Song, T., Zhou, P., Liu, Z., Hu, B., Ji, D., Wang, L., Zhu, X., Yan, C., Ehn, M., Gao, W., Pan, Y., Xin, J., Sun, Y., Kerminen, V.-M., Kulmala, M. and Petäjä, T.: Rapid formation of intense haze episodes via aerosol–boundary layer feedback in Beijing, Atmos. Chem. Phys., 20(1), 45–53, doi:10.5194/acp-20-45-2020, 2020d.

Wang, Y. H., Hu, B., Ji, D. S., Liu, Z. R., Tang, G. Q., Xin, J. Y., Zhang, H. X., Song, T., Wang, L. L., Gao, W. K., Wang, X. K. and Wang, Y. S.: Ozone weekend effects in the Beijing-Tianjin-Hebei metropolitan area, China, Atmos. Chem. Phys, 14, 2419–2429, doi:10.5194/acp-14-2419-2014, 2014c.

Wang, Y. H., Liu, Z. R., Zhang, J. K., Hu, B., Ji, D. S., Yu, Y. C. and Wang, Y. S.: Aerosol physicochemical properties and implications for visibility during an intense haze episode during winter in Beijing, Atmospheric Chemistry and Physics, 15(6), 3205–3215, doi:10.5194/acp-15-3205-2015, 2015.

Wu, Z., Wang, Y., Tan, T., Zhu, Y., Li, M., Shang, D., Wang, H., Lu, K., Guo, S., Zeng, L. and Zhang, Y.: Aerosol Liquid Water Driven by Anthropogenic Inorganic Salts: Implying Its Key Role in Haze Formation over the North China Plain, Environmental Science and Technology Letters, 5(3), 160–166, doi:10.1021/acs.estlett.8b00021, 2018.

Xie, Y., Ding, A., Nie, W., Mao, H., Qi, X., Huang, X., Xu, Z., Kerminen, V. M., Petäjä, T., Chi, X., Virkkula, A., Boy, M., Xue, L., Guo, J., Sun, J., Yang, X., Kulmala, M. and Fu, C.: Enhanced sulfate formation by nitrogen dioxide: Implications from in-situ observations at the SORPES station, Journal of Geophysical Research, 120(24), 12,679-12,694, doi:10.1002/2015JD023607, 2015.

Xue, J., Yuan, Z., Griffith, S. M., Yu, X., Lau, A. K. H. and Yu, J. Z.: Sulfate Formation Enhanced

by a Cocktail of High NOx, SO2, Particulate Matter, and Droplet pH during Haze-Fog Events in Megacities in China: An Observation-Based Modeling Investigation, Environmental Science and Technology, 50(14), 7325–7334, doi:10.1021/acs.est.6b00768, 2016.

Xue, J., Yu, X., Yuan, Z., Griffith, S. M., Lau, A. K. H., Seinfeld, J. H. and Yu, J. Z.: Efficient control of atmospheric sulfate production based on three formation regimes, Nature Geoscience, 12(12), 1–6, doi:10.1038/s41561-019-0485-5, 2019.

Zheng, B., Tong, D., Li, M., Liu, F., Hong, C., Geng, G., Li, H., Li, X., Peng, L., Qi, J., Yan, L., Zhang, Y., Zhao, H., Zheng, Y., He, K. and Zhang, Q.: Trends in China's anthropogenic emissions since 2010 as the consequence of clean air actions, Atmospheric Chemistry and Physics Discussions, 1–27, doi:10.5194/acp-2018-374, 2018.

Zhong, J., Zhang, X., Dong, Y., Wang, Y., Liu, C., Wang, J., Zhang, Y. and Che, H.: Feedback effects of boundary-layer meteorological factors on cumulative explosive growth of PM2.5 during winter heavy pollution episodes in Beijing from 2013 to 2016, Atmospheric Chemistry and Physics, 18(1), 247–258, doi:10.5194/acp-18-247-2018, 2018.

Zhou, Y., Dada, L., Liu, Y., Fu, Y., Kangasluoma, J., Chan, T., Yan, C., Chu, B., Daellenbach, K. R., Bianchi, F., Kokkonen, T. V., Liu, Y., Kujansuu, J., Kerminen, V.-M., Petäjä, T., Wang, L., Jiang, J. and Kulmala, M.: Variation of size-segregated particle number concentrations in wintertime Beijing, Atmospheric Chemistry and Physics, 20(2), 1201–1216, doi:10.5194/acp-20-1201-2020, 2020.

423

424

425

426

427

428

429

430

431

432

434

435
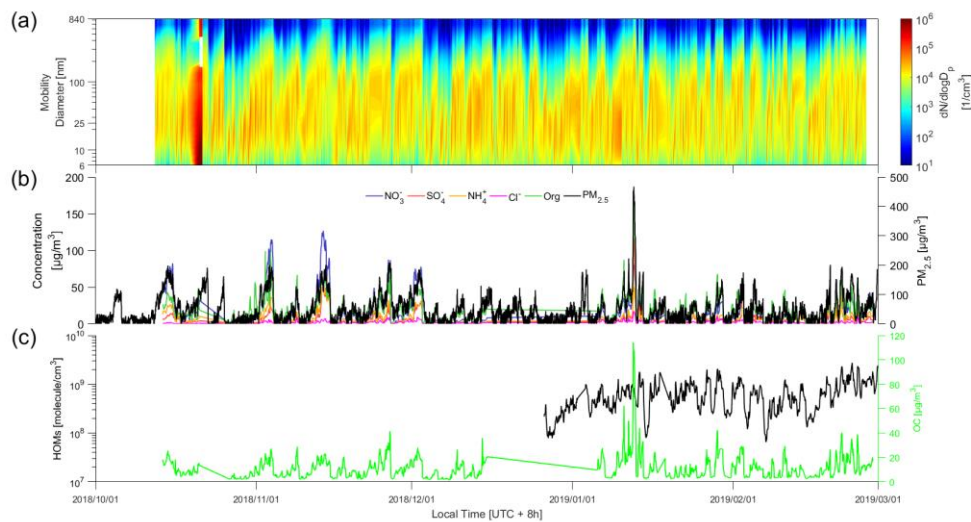
Figure 1. Time series of (a) particle number concentration distribution (PNSD) from 6 nm to 840 nm (b) chemical composition of NR_PM$_{2.5}$ and PM$_{2.5}$ mass concentrations (c) The concentrations of organic carbon (OC) and highly oxygenated organic molecules (HOM).

439

440

441

442

443

444

445

446

447

448

449

450

451

452

453

454

455

456

457
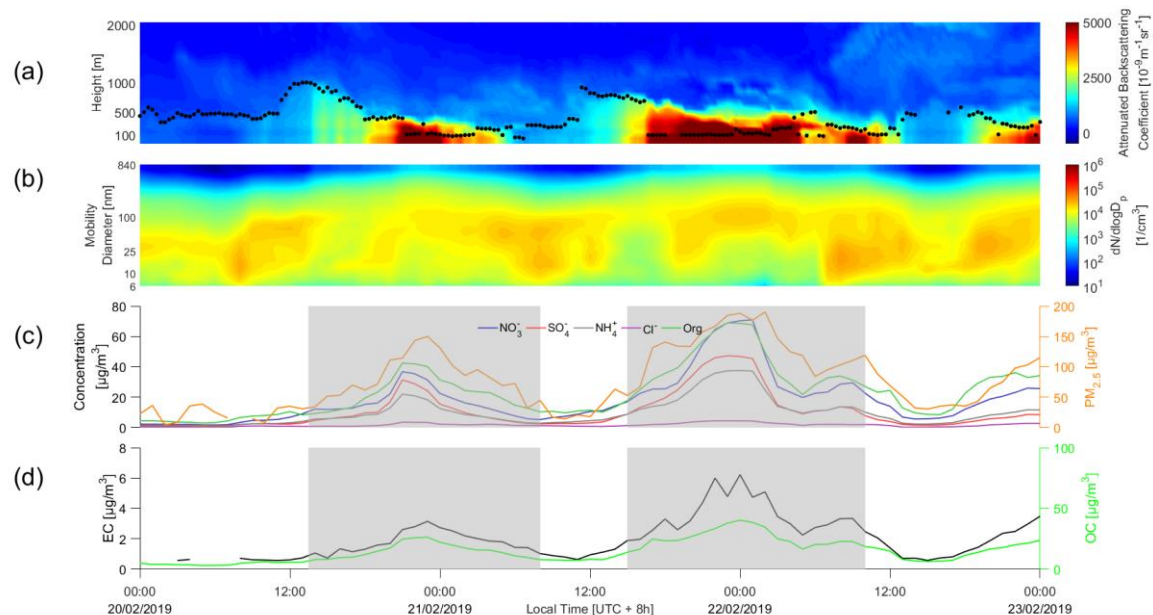
Figure 2. Time series of (a) attenuated backscattering coefficient and mixing layer height (b) particle

number concentration distribution (PNSD), (c) chemical composition and PM$_{2.5}$ mass concentrations

and (d) elemental carbon (EC) and organic carbon (OC). The haze periods are marked by the shaded

areas.

462

463

464

465

466

467

468

469

470

471

472

473

474
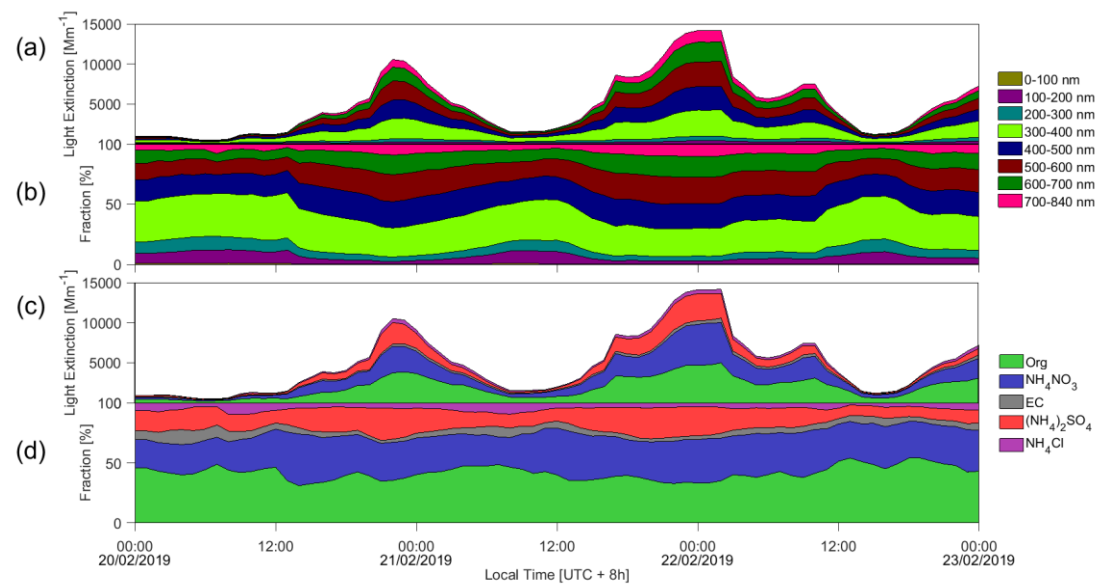
Figure 3. Time series of (a, b) variation of light extinction from different size aerosol and fractions,

and (c, d) variation of light extinction from different aerosol species and fractions. The legends in the

left side of figures are particle diameter and the right side are chemical compositions, respectively.

478

479

480

481

482

483

484

485

486

487

488

489
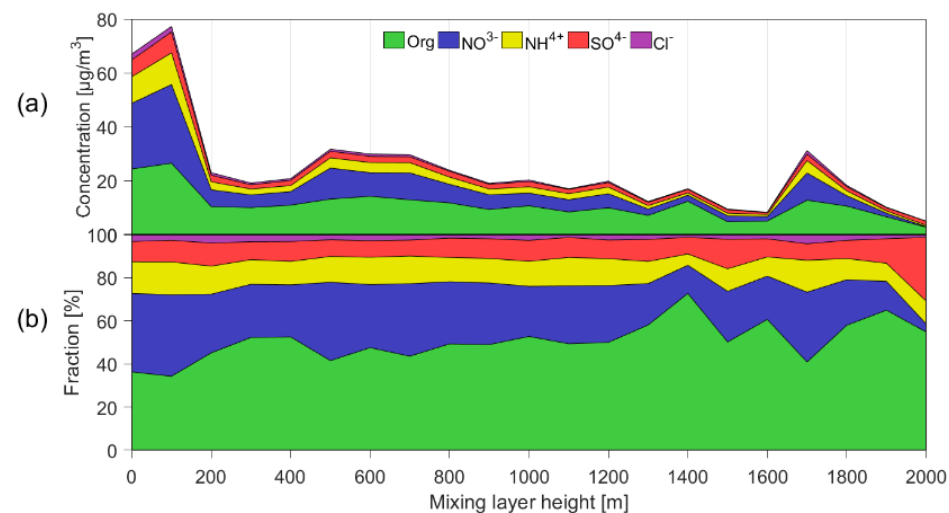
Figure 4. Statistical relationship between MLH and concentration (a) and fraction (b) of chemical

composition species. Only daytime conditions determined by ceilometer from non-rainy periods

(RH<95%) during the observation (~ 6 months) are considered.

493

494

495

496

497

498

499

500

501

502

503

504
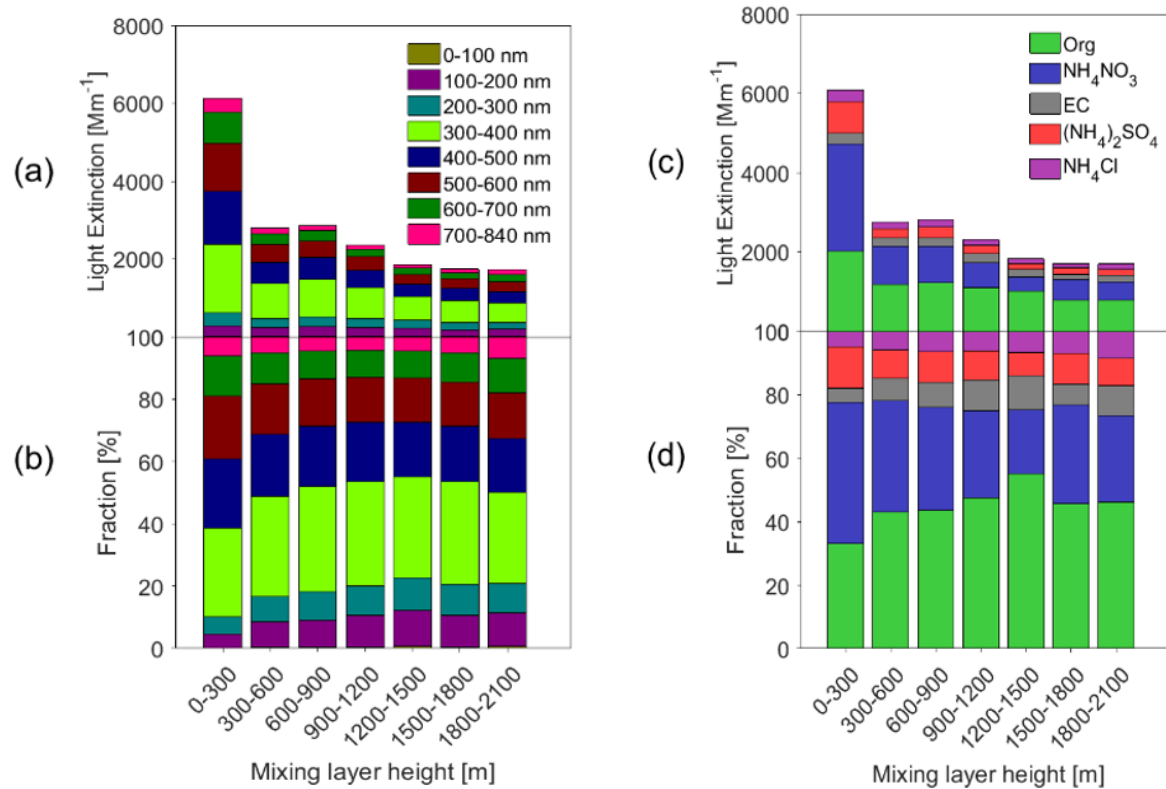
Figure 5. Statistical relationship between MLH and light extinction of different aerosol species. Only

daytime conditions determined by the ceilometer from non-rainy periods (RH<95%) are considered.

521

522

523

524

525

526

527

528

529

530

531
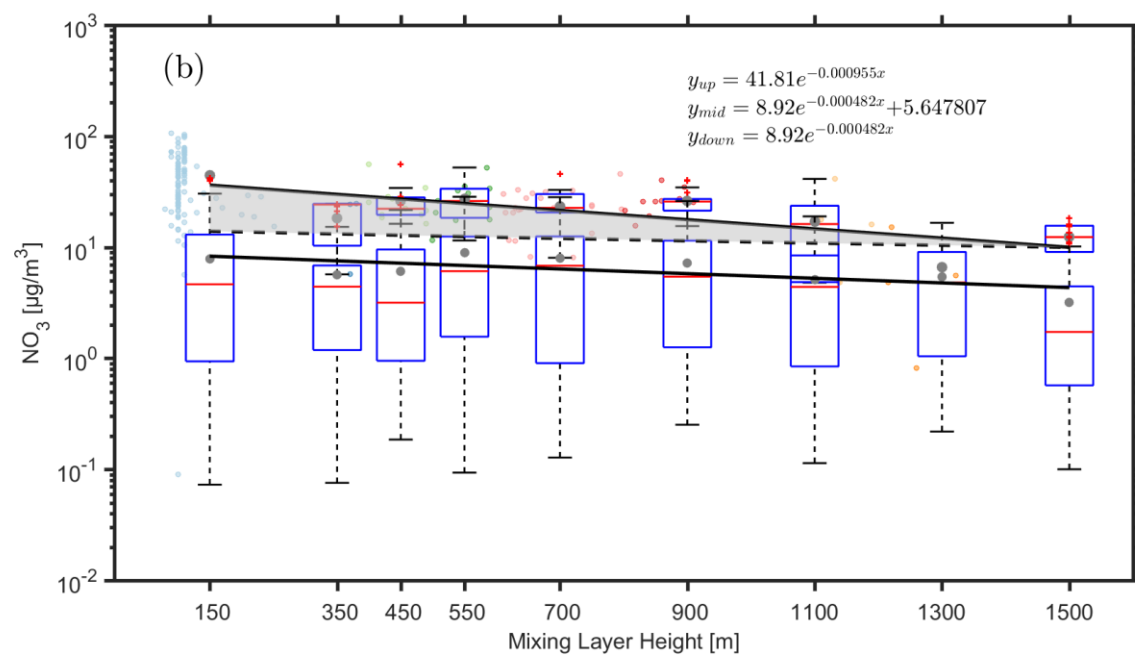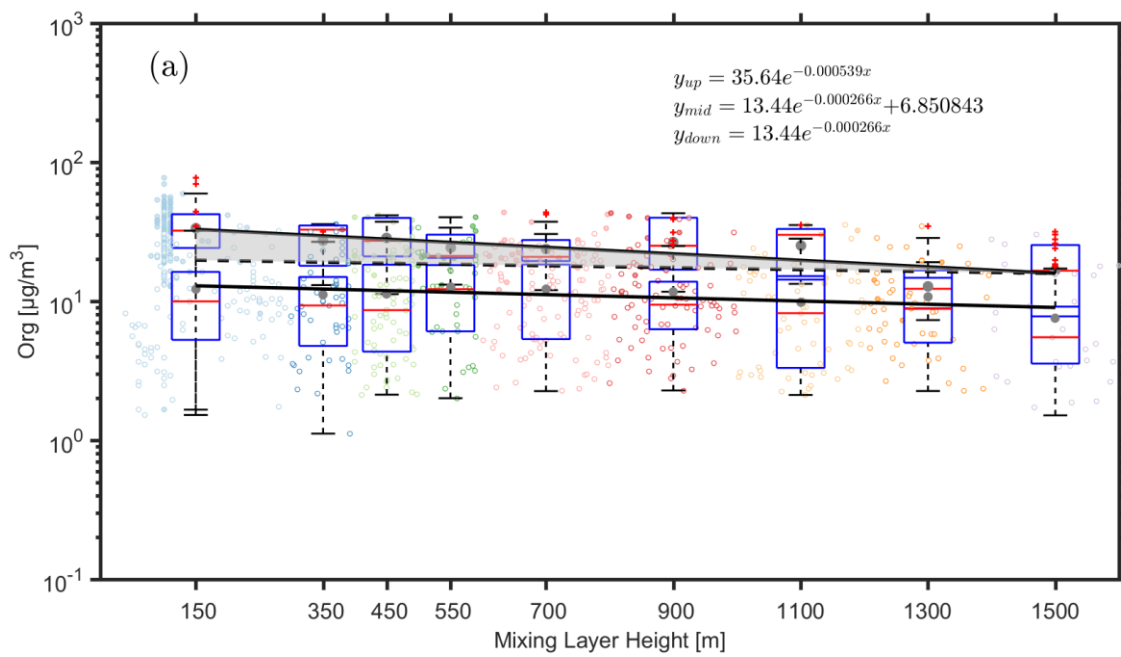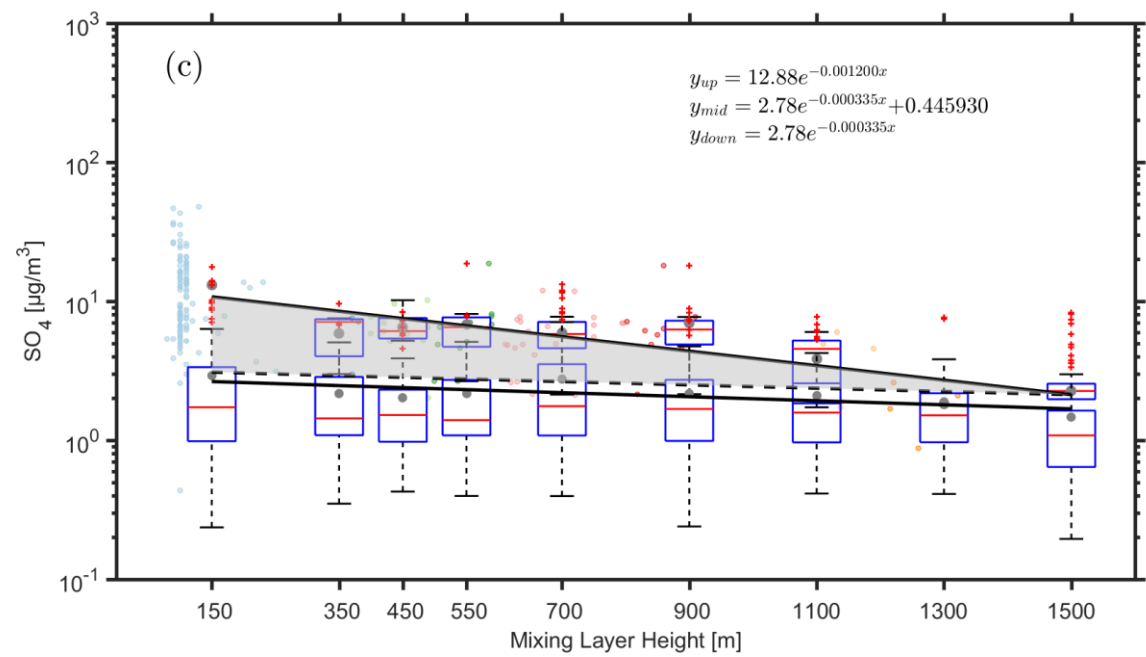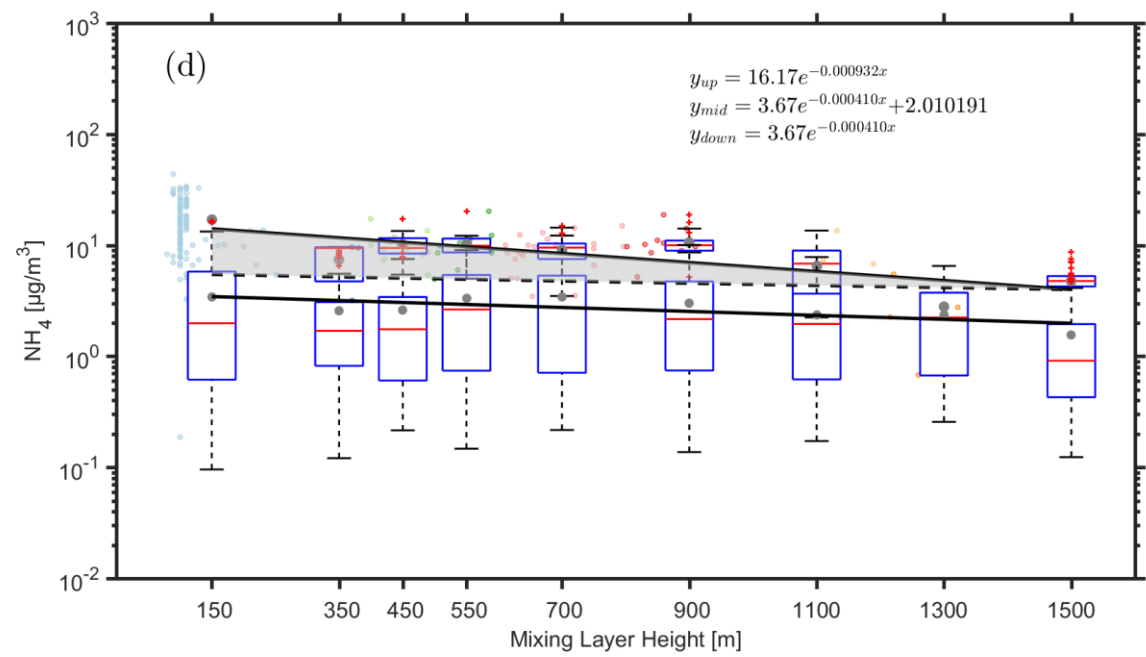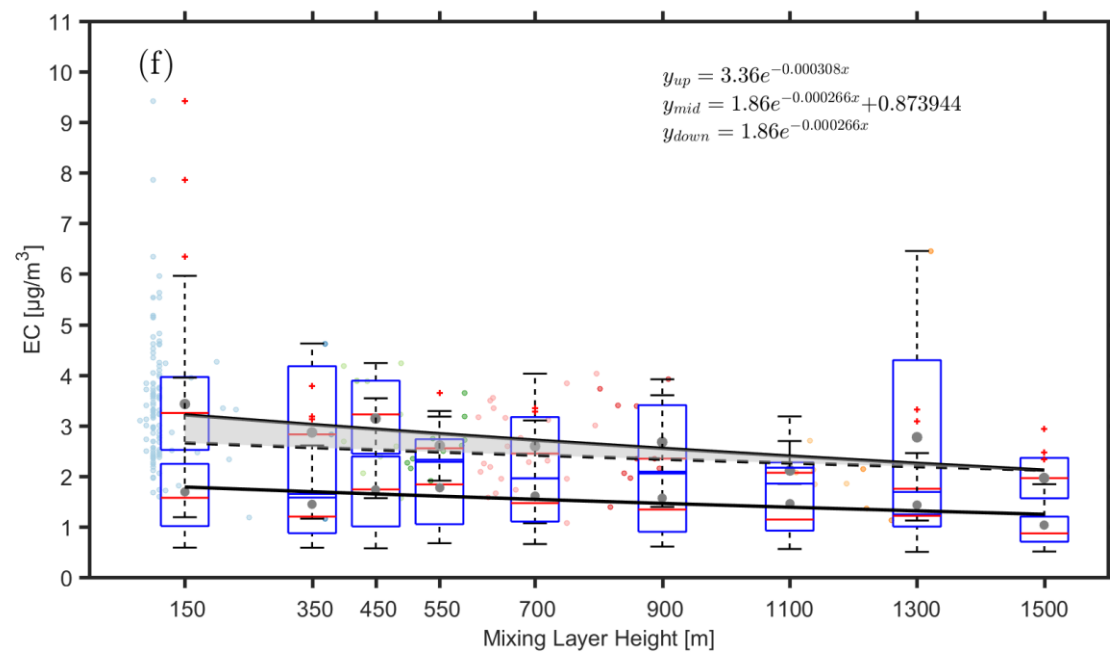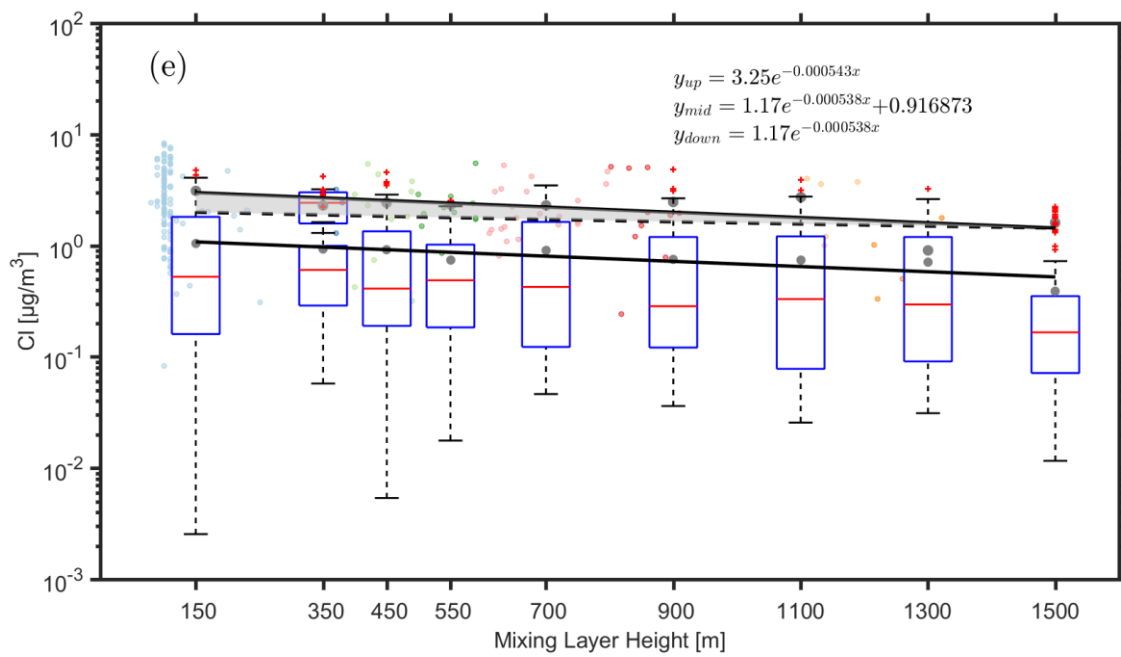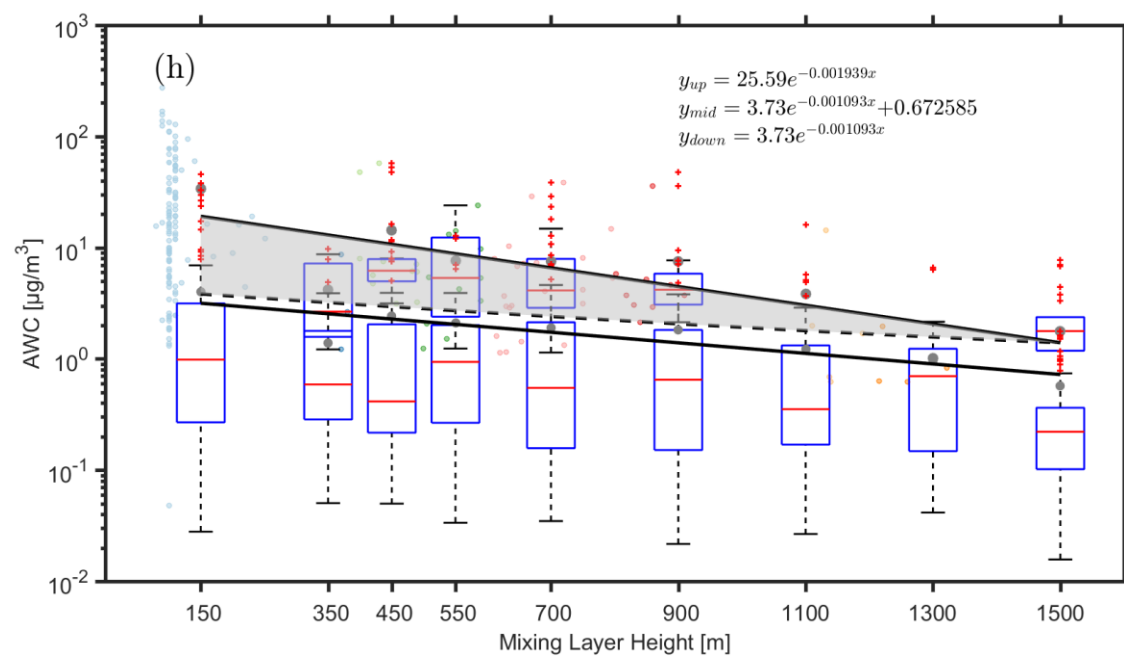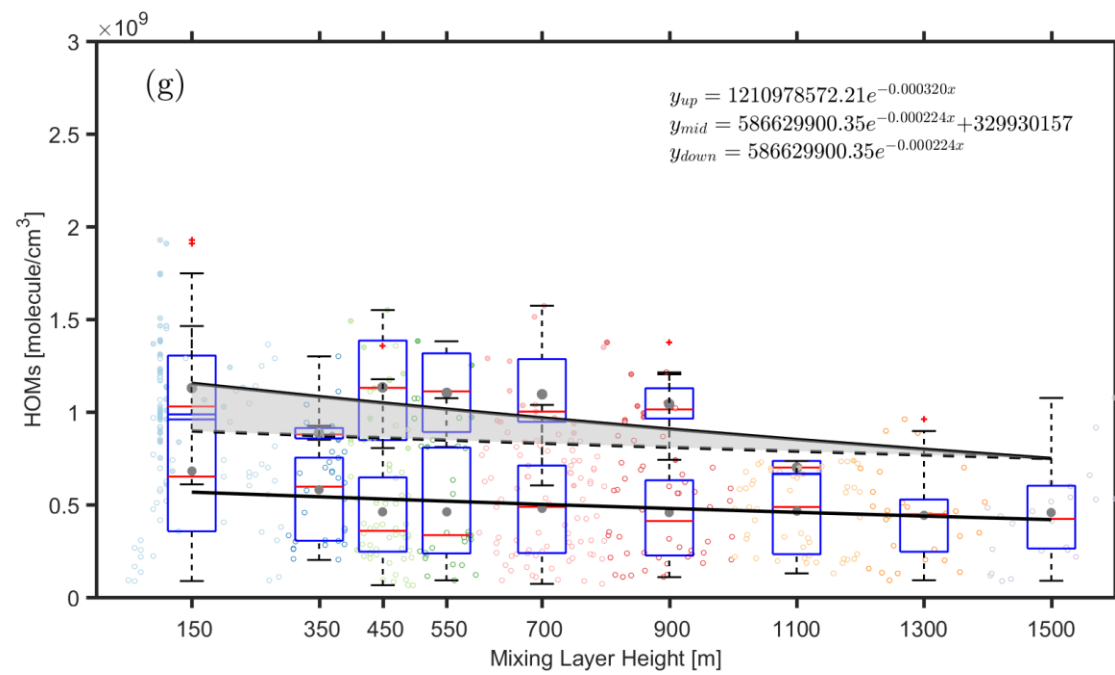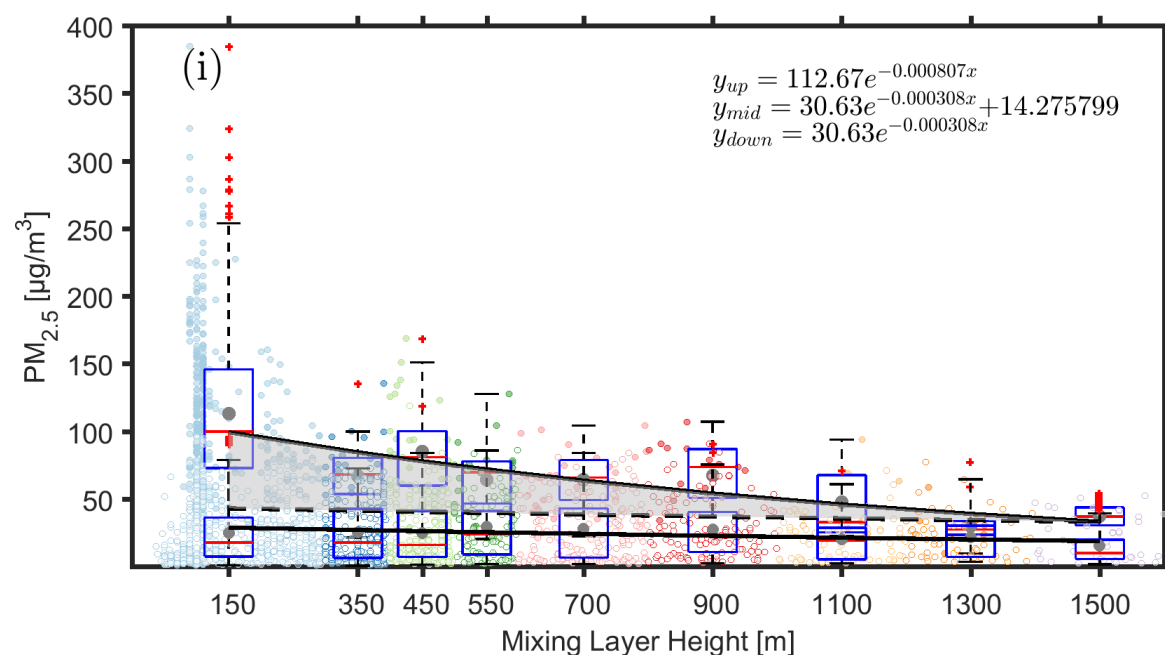
Figure 6. Observed dependency of (organics (a), nitrate (b), ammonium (c), sulfate (d), chlorine (e), element carbon (f), HOMs (g), AWC (h) and $PM_{2.5}$(i) on the MLH during polluted and less-polluted conditions. The data related to the upper fitting line represents $PM_{2.5}$ concentrations larger than 75 μg m^{-3}, while the date related to the lower fitting line represents $PM_{2.5}$ concentrations lower than 75 μg m^{-3}. Only daytime conditions determined by the ceilometer from non-rainy periods (RH<95%) were considered. The solid cycles and hollow cycles denotes concentrations that are more than 75 μg m^{-3} and less than 75 μg m^{-3}, respectively. The dark grey points and red lines in the boxes represent mean and median values, respectively. The shaded area between the upper solid and dotted lines corresponds to an increased amount of the specific compounds with decreased MLH, assuming that the compound has the same variation pattern under highly- polluted conditions as in less polluted time.

551

552

553
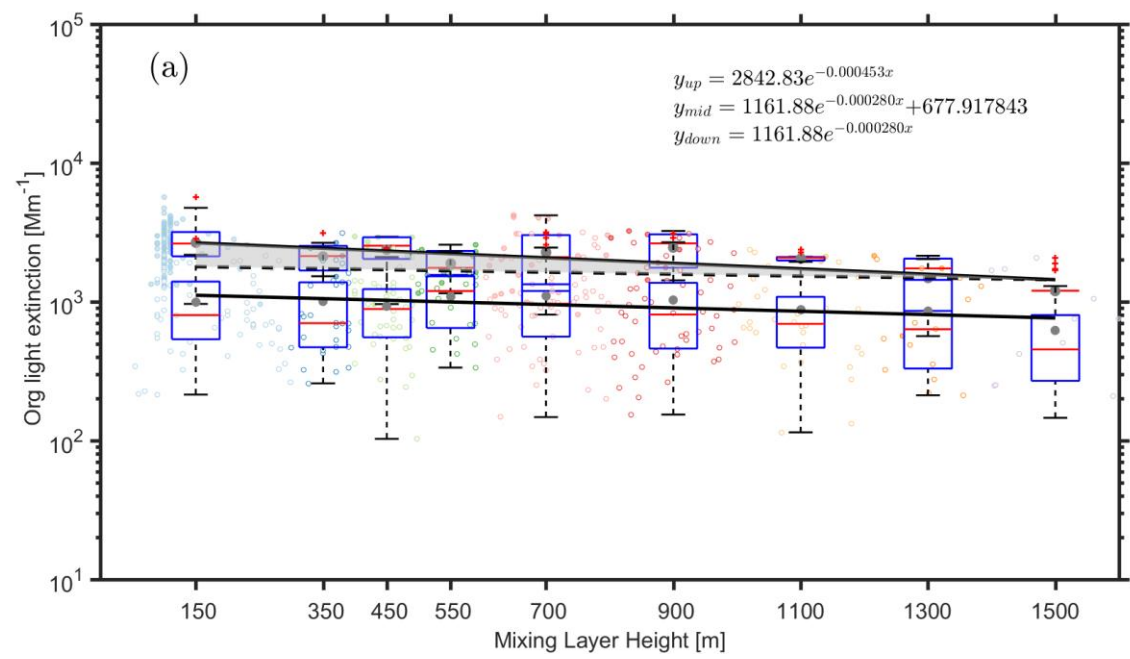
554
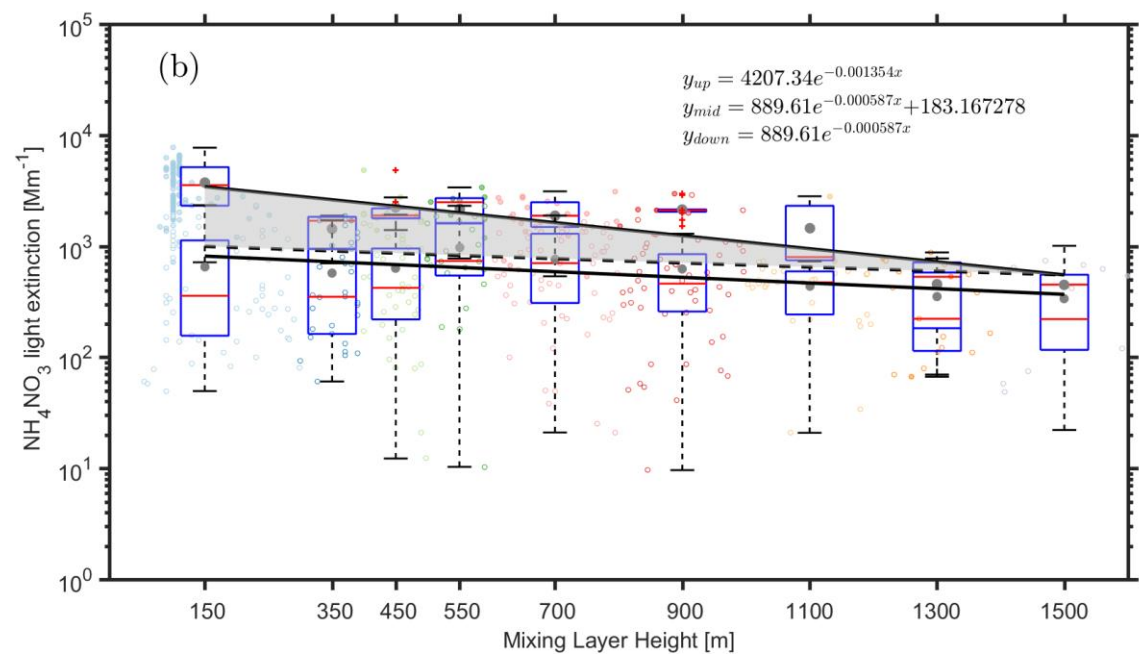
555

556
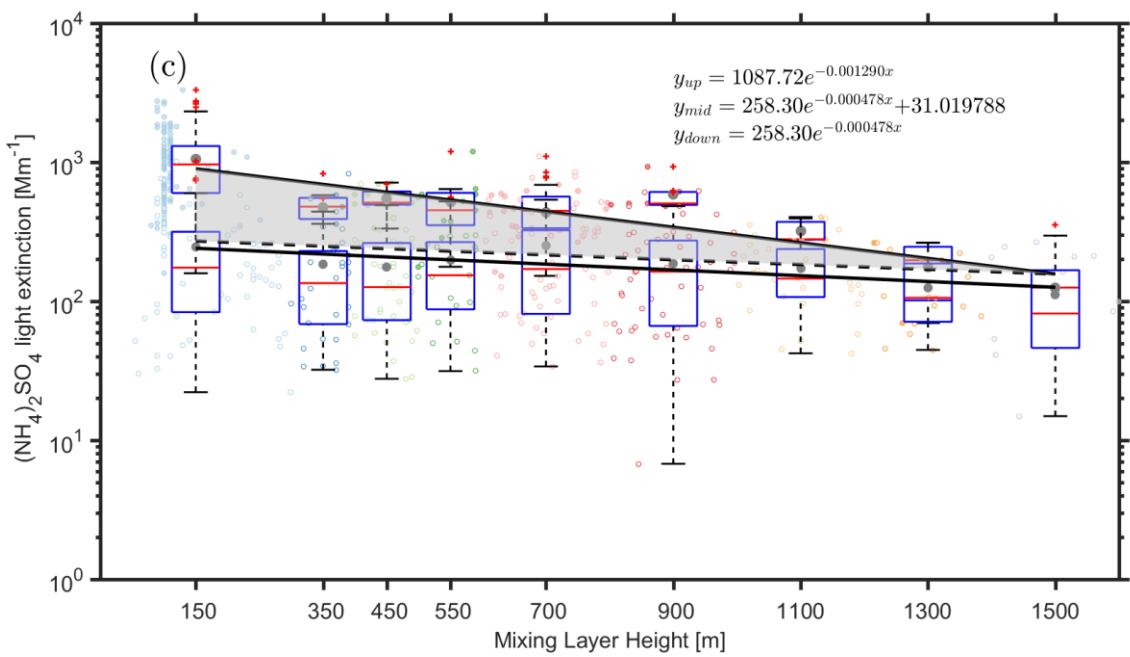
557
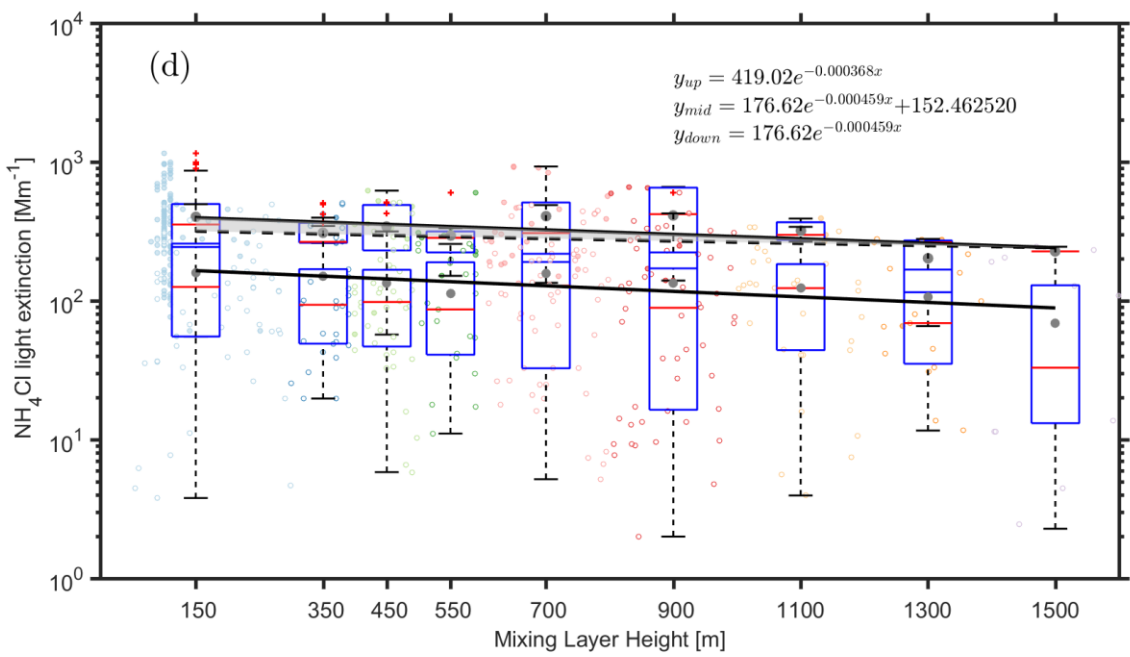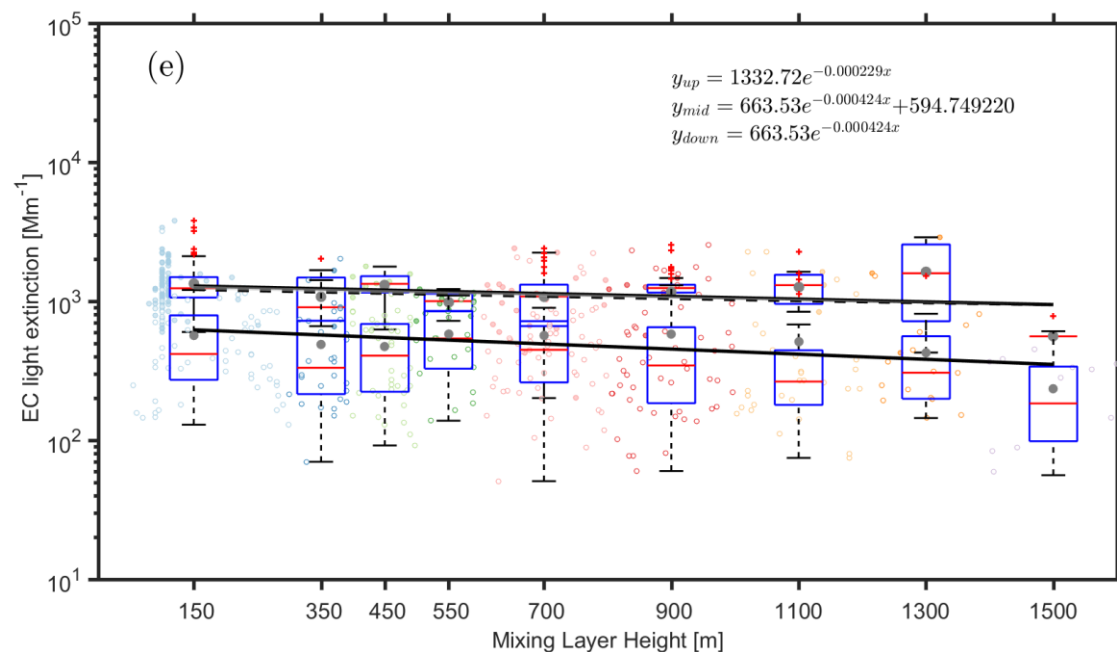
Figure 7. Observed dependency of the aerosol light extinction due to NH_4NO_3 (a) $(NH_4)_2SO_4$ (b), NH_4Cl (c) Org (d) and EC (e) on the MLH during polluted and non-polluted conditions. The data related to the upper fitting line represents $PM_{2.5}$ concentrations larger than 75 μg m^{-3}, while the date related to the lower fitting line represents $PM_{2.5}$ concentrations less than 75 μg m^{-3}. Only daytime conditions determined by ceilometer from non-rainy periods (RH<95%) are considered. The dark grey points and red lines in the boxes represent mean and median values, respectively. The shaded area between the upper solid and dashed line corresponds to an increased amount of $PM_{2.5}$ with a decreased MLH, assuming that $PM_{2.5}$ has the same variation pattern under highly- polluted conditions as in less polluted time

580
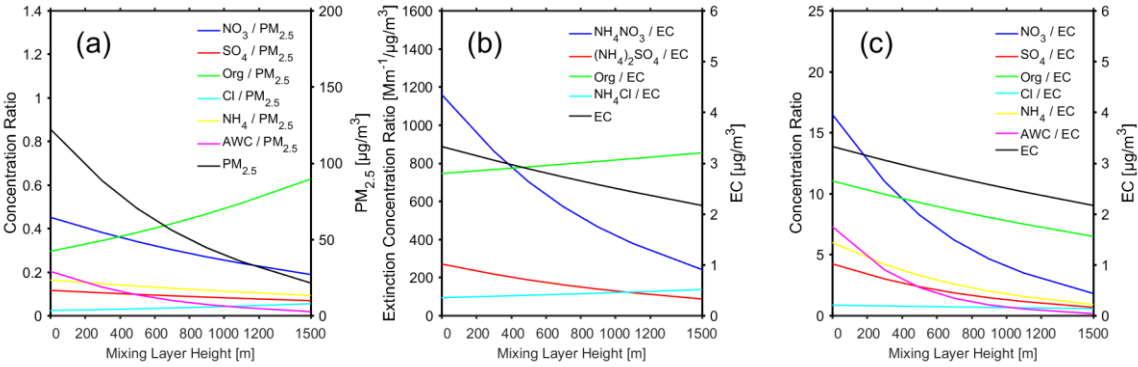
Figure 8. (a) the ratio of the mass concentration of different chemical components (nitrate, sulfate, organics, chlorine, ammonium) and AWC to the mass concentration of NR_PM$_{2.5}$ as a function of MLH. (b) the ratio of dry aerosol light extinction by different chemical components (NH$_4$NO$_3$, (NH$_4$)$_2$SO$_4$, Org, NH$_4$Cl) to the mass concentration EC as a function of MLH (c) the ratio of the mass concentration of different chemical components (nitrate, sulfate, organics, chlorine, ammonium) and AWC to the mass concentration of EC as a function of MLH. All the date corresponds to polluted conditions (fine PM >75 μg m^{-3}), and only daytime conditions determined by the ceilometer from non-rainy periods (RH<95%) were considered.

589

590

591

592

593

594

595

596

597

598

599

600

601

602

603
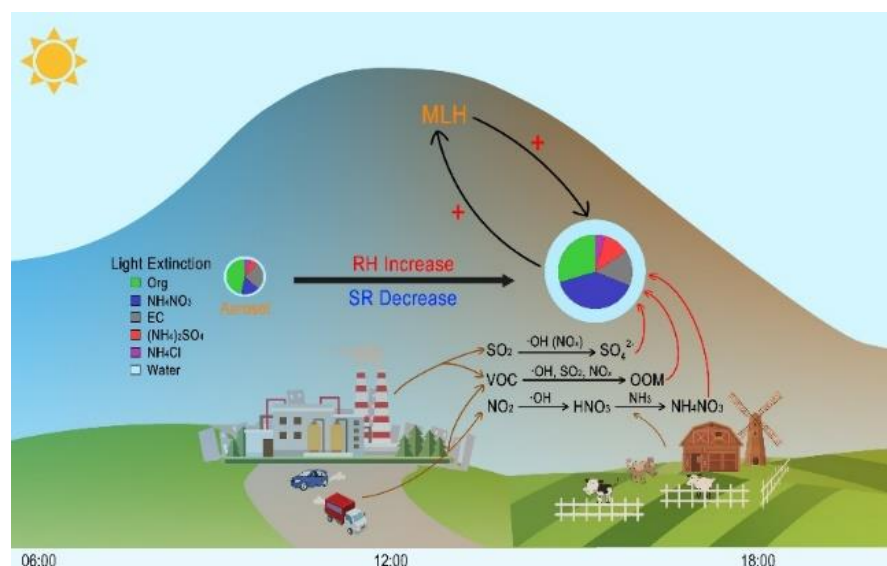
Figure 9. **A schematic picture illustrating the process of rapid aerosol mass growth and enhanced light extinction in Beijing**. The plus symbols represent the strengthening of a specific process. At the presence of aerosols during afternoon time in Beijing, the intensity of solar radiation reaching the surface will be decreased and relative humidity will be increased. As a result, the development of boundary layer will be suppressed, and the concentrations of aerosol precursors (e.g., SO_2, NO_2, VOC) will be increased. In turn, the secondary production of these sulfate, nitrate and oxygenated organic compounds will be enhanced due to increased concentrations and partitioning of these compounds into the aerosol phase. The increased formation of secondary aerosol mass will reduce solar radiation further and the haze formation increased, as shown in pie charts that the light extinction fraction of aerosol changed from organic to nitrate. Noting that during intensive haze periods, nitrate and its contribution to light extinction contribution increased dramatically.

615

616

617

618

619